

Four-Beam Model for Vibration Analysis of a Cantilever Beam with an Embedded Horizontal Crack

LIU Jing^{1,2,3}, ZHU Weidong³, CHARALAMBIDES Panos G³, SHAO Yimin^{1,*},
XU Yongfeng³, WU Kai³, and XIAO Huifang⁴

1 State Key Laboratory of Mechanical Transmission, Chongqing University, Chongqing 400030, China

2 College of Mechanical Engineering, Chongqing University, Chongqing 400030, China

3 Department of Mechanical Engineering, University of Maryland, Baltimore County, Baltimore, MD 21250, USA

4 National Engineering Research Center of Flat Rolling Equipment, University of Science and Technology Beijing, Beijing 100083, China

Received February 8, 2015; revised August 18, 2015; accepted September 1, 2015

Abstract: As one of the main failure modes, embedded cracks occur in beam structures due to periodic loads. Hence it is useful to investigate the dynamic characteristics of a beam structure with an embedded crack for early crack detection and diagnosis. A new four-beam model with local flexibilities at crack tips is developed to investigate the transverse vibration of a cantilever beam with an embedded horizontal crack; two separate beam segments are used to model the crack region to allow opening of crack surfaces. Each beam segment is considered as an Euler-Bernoulli beam. The governing equations and the matching and boundary conditions of the four-beam model are derived using Hamilton's principle. The natural frequencies and mode shapes of the four-beam model are calculated using the transfer matrix method. The effects of the crack length, depth, and location on the first three natural frequencies and mode shapes of the cracked cantilever beam are investigated. A continuous wavelet transform method is used to analyze the mode shapes of the cracked cantilever beam. It is shown that sudden changes in spatial variations of the wavelet coefficients of the mode shapes can be used to identify the length and location of an embedded horizontal crack. The first three natural frequencies and mode shapes of a cantilever beam with an embedded crack from the finite element method and an experimental investigation are used to validate the proposed model. Local deformations in the vicinity of the crack tips can be described by the proposed four-beam model, which cannot be captured by previous methods.

Keywords: cracked cantilever beam, embedded horizontal crack, transverse vibration, four-beam model, continuous wavelet transform

1 Introduction

Beam structures are one of the most widely used types of components or structures in industry and play an important role in system performance. As one of the major failure modes of beam structures due to periodic loads, embedded cracks in them can significantly affect their dynamic characteristics, and cause catastrophic failures and accidents in industry. Hence it is important to investigate the dynamic characteristics of a beam structure with an embedded crack for early crack detection and diagnosis for industrial maintenance purposes.

It is well known that dynamic characteristics of beam

structures are correlated with their modal parameters, such as natural frequencies, mode shapes, and damping ratios, which can be changed when there are cracks in them^[1-2]. An investigation on the changes in the dynamic characteristics makes it possible to detect and diagnose cracks in beam structures, and different methods have been presented^[1-4]. Modeling and simulation methods can provide an accurate and comprehensive method for predicting the dynamic characteristics of cracked beam structures, which can also provide some guidance to early crack detection and diagnosis in these structures. Much research work has been conducted in this area, and many methods have been developed to model cracks in beam structures. A crack has been modeled by a rotational spring, an elastic hinge, a cut-out, a pair of concentrated couples, or a zone with a reduced elastic modulus^[5]. The most popular models of cracks in beam structures are rotational spring models.

YUEN^[6] investigated the relationship between the crack location and size and the changes in the eigenvalues and eigenvectors of a cracked cantilever beam using a finite

* Corresponding author. E-mail: ymshao@cqu.edu.cn

Supported by National Natural Science Foundation of China(Grant Nos. 51035008, 51304019), National Science Foundation of USA(Grant Nos. CMMI-1000830, CMMI-1229532), the University of Maryland Baltimore County Directed Research Initiative Fund Program, and Fundamental Research Funds for the Central Universities, China(Grant No. FRF-TP-14-123A2)

element(FE) method. RIZOS and ASPRAGATHOS^[7] proposed a method to model a crack as a localized flexibility and used measured amplitudes of a mode shape of a cantilever beam to identify the location and size of an edge crack. Their method requires amplitude measurements at two locations along the beam. NANDWANA and MAITI^[8] modeled an edge crack as a rotational spring and used a semi-analytical method to identify the location and size of a crack in a cantilever beam based on changes in its natural frequencies. KISA^[9] investigated the effects of cracks on the dynamic characteristics of a cantilever composite beam using FE and component mode synthesis methods. The crack sections divide the beam into several parts, which are connected by rotational springs. NAHVI and JABBARI^[10] proposed an experimental method and a FE method to identify the location and size of an edge crack in a cantilever beam based on changes in its natural frequencies and mode shapes. LIN and CHANG^[11] developed an analytical method to investigate the dynamic response of a cantilever beam with an edge crack subjected to a concentrated moving load. The crack is also modeled as a rotational spring in their model. YANG and CHEN^[12] proposed a theoretical investigation on the free vibration and elastic buckling of a cantilever beam with edge cracks based on Euler-Bernoulli beam theory. They also used a rotational spring model to describe the effects of the cracks. SEYEDPOOR^[13] developed a two-stage method to identify the locations and extent of multiple damage in beam structures based on numerical results from a FE model. The effect of a crack is simulated through a relative reduction of the elastic modulus of each element. LU, et al^[14], proposed a two-step approach to identify the location and size of an edge crack in a cantilever beam using changes in its mode shape curvatures and a response sensitivity analysis. They used a localized stiffness reduction to model the effect of the crack in the beam.

OSTACHOWICZ and KRAWZUK^[3] investigated a continuous model of a cracked cantilever beam. Two edge cracks were modeled by two rotational springs; the model was used to study the effects of two edge cracks on the natural frequencies of the cracked cantilever beam. SHIFRIN and RUOTOLO^[15] used a continuous mathematical model to calculate the natural frequencies of a cantilever beam with an arbitrary number of edge cracks. They used massless springs to model the cracks in the beam. LIN, et al^[16], developed a theoretical model of an Euler-Bernoulli beam with an arbitrary number of edge cracks using the transfer matrix method. The cracks were modeled using the method in Ref. [3]. KHIEM and LIEN^[17] used a dynamic stiffness matrix method to identify the locations and sizes of cracks in a cantilever beam based on changes in its natural frequencies. They also used a spring model to represent the cracks. CHANG and CHEN^[18] developed a technique to detect the locations and sizes of cracks in a cantilever beam using a spatial wavelet-based method. The cracks were also modeled by rotational

springs. PATIL and MAITI^[19] developed a method to identify the locations and sizes of cracks in a cantilever beam based on changes in its natural frequencies. Their analysis is based on an energy method and the representation of a crack by a rotational spring. MORADI and KARGOZARFARD^[20] developed an evolutionary algorithm to identify cracks in a cantilever beam based on changes in its natural frequencies and some strain energy parameters. Each crack was modeled by a rotational spring.

The above literature shows that most of the previous works are focused on edge cracks in a cantilever beam. Some researchers have studied a closed, embedded horizontal crack or a delamination in a beam^[21–31]. MAJUMDAR and SURYANARAYAN^[23] developed an analytical model of a beam with through-width delaminations parallel to the beam surfaces, which are arbitrarily located in both the spanwise and thicknesswise directions. In their model, three beam segments are used to model the beam with a delamination, and each beam segment is considered as an Euler-Bernoulli beam. They used continuity of transverse displacements, slopes, bending moments, shear forces, and axial displacements and forces to describe the effect of the delamination in the beam. TRACY and PARDOEN^[24] proposed a methodology for predicting natural frequencies, mode shapes, and modal damping of a composite beam and relating them to a delamination based on laminate mechanics. It was assumed that there are relative in-plane and out-of-plane motions between delaminated sublaminates. The induced discontinuity at an end of a delamination is considered as an additional degree of freedom. ISHAK, et al^[25], investigated wave propagation in an infinitely-long beam with an embedded horizontal crack, and used a multilayer perception network to identify the length, depth, and location of the crack. The beam segment containing the crack is modeled by a reduced bending stiffness. Some studies^[26–30] are also focused on modeling of the delamination in a laminated material. The matching conditions at the junctions are formulated as changes in the axial forces and bending moments in Refs. [25–30], which cannot describe rotational flexibilities of cross-sections of the beam at the crack tips due to the presence of a crack. QIAO and CHEN^[31] used the model in Ref. [32] to study the tip deformations of the delaminations in a flexible joint for a clamped-clamped and a simple supported bi-layer composite beam with an interface delamination. LI, et al^[33], proposed an analytical method to calculate the local flexibility and rotational spring stiffness cause by a crack in a I-beam. They^[34] proposed a three-step-meshing method for multiple cracks identification in a cracked cantilever beam. YAZDI and SHOOSHTARI^[35] proposed a novel FE with a central crack for fracture applications. CHU, et al^[36], extended the double cantilever beam model to functionally graded material according to two-dimensional(2D) theory of elasticity. NANDAKUMAR and SHANKAR^[37] proposed a novel structural damage detection scheme using

transfer matrix for the local crack identification in large structures.

In this paper, a new four-beam model with local flexibilities at crack tips is developed to investigate the transverse vibration of a cantilever beam with an embedded horizontal crack. Such a crack can occur in a layered structure prone to delamination. While the beam is assumed to be homogeneous here, the methodology developed in this work can be extended to laminates with homogeneous layers. Two separate beam segments are used here to model the crack region so that crack surfaces are allowed to open. The proposed model can describe effects of local deformations in the vicinity of crack tips, which cannot be captured by previous methods in the literature. Each beam segment is assumed to be an Euler-Bernoulli beam. Compliances at the crack tips are analytically calculated partly based on the results in Ref. [38]. The governing equations and the matching and boundary conditions of the beam segments are derived using Hamilton's principle. The natural frequencies and mode shapes of the cracked cantilever beam are calculated using the transfer matrix method. The effects of the crack length, depth, and location on the first three natural frequencies and mode shapes of the cracked cantilever beam are investigated. A continuous wavelet transform(CWT) method^[39] is used to process the mode shapes of the cracked cantilever beam. Sudden changes in spatial variations of the wavelet coefficients are observed; they can be used to identify the length and location of an embedded horizontal crack. Because the FE method has been widely used in deformation and vibration studies of beams with cracks^[40-44], the results from the proposed model are verified using commercial FE software^[45]. An experimental investigation is also undertaken to validate the proposed model. This work is a first step in modeling and detecting a slant crack in a beam structure.

2 Free Vibration Analysis of a Cantilever Beam with an Embedded Horizontal Crack

2.1 Four-beam model with local flexibilities at crack tips

A uniform Euler-Bernoulli cantilever beam of length L , height h , and width b with an embedded horizontal crack of length $2a$ is shown in Fig. 1, where P is an applied force used to calculate crack-induced rotational flexibilities of cross-sections of the beam at the crack tips, X_0 and X_3 are the positions of the fixed and free ends of the beam in the global XY coordinate system, respectively, and X_1 and X_2 are the beginning and end positions of the crack, respectively. The crack length is $2a$ and the crack depth from the top surface of the beam is h_1 with $0 < h_1 < h$. It is assumed that the center of the crack is located at X_c with $L_2/2 < X_c < L - L_2/2$. The beam is divided into four segments of lengths L_1 , L_2 , L_3 , and L_4 , respectively, with $L_2 = L_3 = 2a$,

as shown in Fig. 1.

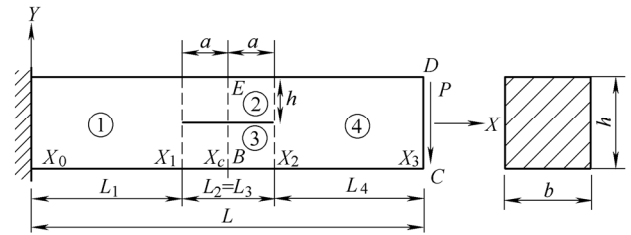


Fig. 1. Schematic of a cantilever beam with an embedded horizontal crack

A four-beam model with local flexibilities at X_1 and X_2 , is developed to describe the cantilever beam with an embedded horizontal crack, as shown in Fig. 2, where C_1 , C_2 , C_3 , and C_4 are compliances at the crack tips; each beam segment is assumed to be an Euler-Bernoulli beam. The transverse displacement of the i th ($i=1, 2, 3, 4$) beam segment is denoted by $Y_i(X, T)$ with $X_{i-1} < X < X_i$.

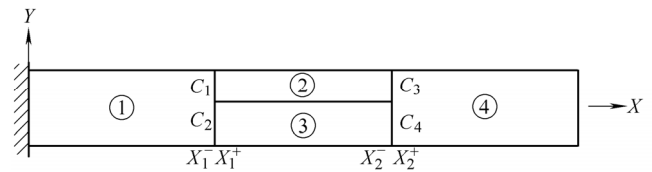


Fig. 2. Schematic of a four-beam model with compliances C_1 , C_2 , C_3 , and C_4 at the crack tips

2.2 Calculation of compliances at the crack tips

According to the analysis in Ref. [38], the total equivalent compliances at X_1 and X_2 are

$$C_l = \frac{ba^3}{3EI[L - (X_c - a)]^2} \left(\frac{h^3}{h_1^3 + (h - h_1)^3} - 1 \right), \quad (1)$$

$$C_r = \frac{ba^3}{3EI[L - (X_c + a)]^2} \left(\frac{h^3}{h_1^3 + (h - h_1)^3} - 1 \right), \quad (2)$$

respectively.

By moment balance of the right parts of beam segments 2 and 3 shown in Fig. 3(c), one has

$$M_{r1} = M_1 + P_1 a, \quad M_{r2} = M_2 + P_2 a, \quad (3)$$

where M_{r1} and M_{r2} are the bending moments at cross-sections X_2^- , as shown in Fig. 2, of beam segments 2 and 3, respectively, and P_1 and P_2 are the shear forces at the same cross-sections of beam segments 2 and 3, respectively.

According to the analysis in Refs. [26, 38], by moment balance of the right part of the beam in Fig. 3(a) at point B , force balance of the right part of the beam in Fig. 3(b) in the X and Y directions, and deflection compatibility of the beam at cross-section X_2^- , which states that the

deflections at cross-section X_2^- relative to those at X_1^+ , as shown in Fig. 2, for beam segments 2 and 3 are the same, one has

$$M_c - M_1 - M_2 + \frac{N_2(h-h_1)}{2} + N_1\left(h - \frac{h_1}{2}\right) = 0,$$

$$N_1 = -N_2, \quad P_1 + P_2 = P,$$

$$\frac{(M_1 + P_1a)(2a)^2}{2EI_2} - \frac{P_1(2a)^3}{3EI_2} = \frac{(M_2 + P_2a)(2a)^2}{2EI_3} - \frac{P_2(2a)^3}{3EI_3}, \quad (4)$$

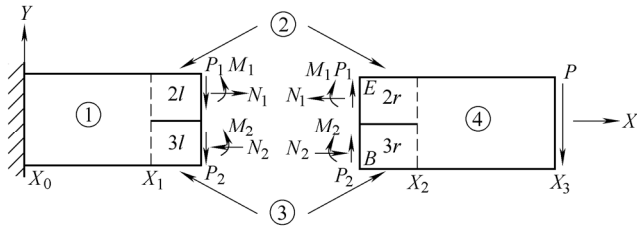
respectively, where $M_c = -P(L - X_c)$, and I_2 and I_3 are cross-sectional area moments of inertia of beam segments 2 and 3, respectively. By Eq. (4), the relationships between P_1 and P_2 , and between M_1 and M_2 , are

$$P_1 = \frac{I_2}{I_2 + I_3} P, \quad P_2 = \frac{I_3}{I_2 + I_3} P, \quad (5)$$

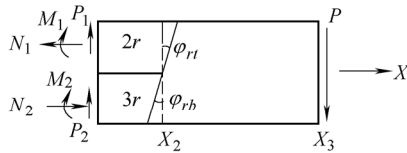
$$M_1 = \frac{I_2 M_c}{I}, \quad M_2 = \frac{I_3 M_c}{I}. \quad (6)$$

Use of Eqs. (4)–(6) in Eq. (3) yields

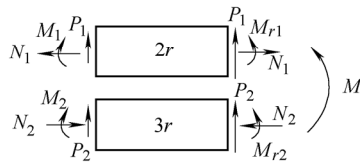
$$\frac{M_{r1}}{M_{r2}} = \frac{M_1 + P_1a}{M_2 + P_2a} = \frac{I_2}{I_3}. \quad (7)$$



(a) Two parts of the cracked cantilever beam divided at the center of the crack



(b) Right part of the cracked cantilever beam



(c) Right parts of beam segments 2 and 3

Fig. 3. Schematic of moment balance and force balance of a cantilever beam

Furthermore, the rotational angles at cross-section X_2^+ , as shown in Fig. 2, relative to those at X_1^+ for beam segments 2 and 3 are the same, one has

$$\frac{2a(M_1 + P_1a)}{EI_2} - \frac{P_1(2a)^2}{2EI_2} + M_{r1}C_3 = \frac{2a(M_2 + P_2a)}{EI_3} - \frac{P_2(2a)^2}{2EI_3} + M_{r2}C_4. \quad (8)$$

Use of Eq. (7) in Eq. (8) yields

$$\frac{C_3}{C_4} = \frac{I_3}{I_2}. \quad (9)$$

By moment balance of beam segment 4 in Fig. 3(b), one has

$$M_r = M_{r1} + M_{r2}, \quad (10)$$

where M_r is the resultant bending moment at cross-section X_2^+ . Equation (10) can be written as

$$\frac{\varphi_r}{C_r} = \frac{\varphi_{r1}}{C_3} + \frac{\varphi_{r2}}{C_4}, \quad (11)$$

where φ_r , φ_{r1} , and φ_{r2} are the rotational angle at cross-section X_2^+ relative to that at X_2^- , and those for beam segments 2 and 3, as shown in Fig. 3, respectively, which are the same, i.e.,

$$\varphi_r = \varphi_{r1} = \varphi_{r2}. \quad (12)$$

Use of Eq. (12) in Eq. (11) yields

$$\frac{1}{C_r} = \frac{1}{C_3} + \frac{1}{C_4}. \quad (13)$$

By Eqs. (9) and (13), one has

$$\frac{1}{C_3} = \frac{I_2}{C_r(I_2 + I_3)}, \quad \frac{1}{C_4} = \frac{I_3}{C_r(I_2 + I_3)}. \quad (14)$$

Similarly, one has

$$\frac{1}{C_1} = \frac{I_2}{C_l(I_2 + I_3)}, \quad \frac{1}{C_2} = \frac{I_3}{C_l(I_2 + I_3)}. \quad (15)$$

It can be seen from Eqs. (2), (14), and (15) that $C_1 > C_3$ and $C_2 > C_4$; C_1 through C_4 increase with the crack length and depth.

2.3 Calculation of natural frequencies and mode shapes of the four-beam model

By Hamilton's principle, the equations of motion of the four beam segments are (see Appendix A for the derivation)

$$\begin{aligned}
\rho A_1 \frac{\partial^2 Y_1(X, t)}{\partial t^2} + EI_1 \frac{\partial^4 Y_1(X, t)}{\partial X^4} &= 0, \quad X_0 < X < X_1, \\
\rho A_2 \frac{\partial^2 Y_2(X, t)}{\partial t^2} + EI_2 \frac{\partial^4 Y_2(X, t)}{\partial X^4} &= 0, \quad X_1 < X < X_2, \\
\rho A_3 \frac{\partial^2 Y_3(X, t)}{\partial t^2} + EI_3 \frac{\partial^4 Y_3(X, t)}{\partial X^4} &= 0, \quad X_1 < X < X_2, \\
\rho A_4 \frac{\partial^2 Y_4(X, t)}{\partial t^2} + EI_4 \frac{\partial^4 Y_4(X, t)}{\partial X^4} &= 0, \quad X_2 < X < L.
\end{aligned} \quad (16)$$

The boundary conditions are

$$Y_1(0, t) = Y_1'(0, t) = 0, \quad Y_4'''(0, t) = Y_4'''(L, t) = 0. \quad (17)$$

The matching conditions at cross-sections X_1 and X_2 are

$$\begin{aligned}
Y_1(X_1^-, t) &= Y_2(X_1^+, t), \\
Y_1(X_1^-, t) &= Y_3(X_1^+, t), \\
Y_4(X_2^+, t) &= Y_2(X_2^-, t), \\
Y_4(X_2^+, t) &= Y_3(X_2^-, t), \\
h^3 Y_1'''(X_1^-, t) &= h_1^3 Y_2'''(X_1^+, t) + (h - h_1)^3 Y_3'''(X_1^+, t), \\
h^3 Y_1''''(X_1^-, t) &= h_1^3 Y_2''''(X_1^+, t) + (h - h_1)^3 Y_3''''(X_1^+, t), \\
h^3 Y_4''(X_2^+, t) &= h_1^3 Y_2''(X_2^-, t) + (h - h_1)^3 Y_3''(X_2^-, t), \\
h^3 Y_4''''(X_2^+, t) &= h_1^3 Y_2''''(X_2^-, t) + (h - h_1)^3 Y_3''''(X_2^-, t),
\end{aligned} \quad (18)$$

$$\begin{aligned}
Y_2'(X_1^+, t) - Y_1'(X_1^-, t) &= C_1 EI_2 Y_2''(X_1^+, t), \\
Y_3'(X_1^+, t) - Y_1'(X_1^-, t) &= C_2 EI_3 Y_3''(X_1^+, t), \\
Y_4'(X_2^+, t) - Y_2'(X_2^-, t) &= C_3 EI_2 Y_2''(X_2^-, t), \\
Y_4'(X_2^+, t) - Y_3'(X_2^-, t) &= C_4 EI_3 Y_3''(X_2^-, t).
\end{aligned} \quad (19)$$

The following nondimensional variables are introduced:

$$\begin{aligned}
y &= \frac{Y}{L}, \quad x = \frac{X}{L}, \quad x_i = \frac{X_i}{L}, \quad l_1 = \frac{L_1}{L}, \quad l_2 = \frac{L_2}{L}, \\
l_3 &= \frac{L_3}{L}, \quad l_4 = \frac{L_4}{L}, \quad h_c = \frac{h_1}{h}, \quad c_1 = \frac{C_1 EI}{Lb^2}, \\
c_2 &= \frac{C_2 EI}{Lb^2}, \quad c_3 = \frac{C_3 EI}{Lb^2}, \quad c_4 = \frac{C_4 EI}{Lb^2}.
\end{aligned} \quad (20)$$

The equations of motion of the four beam segments in Eq. (16) become

$$\begin{aligned}
\frac{EI_1}{L^4} \frac{\partial y_1^4(x, t)}{\partial x^4} + \rho A_1 \frac{\partial^2 y_1(x, t)}{\partial t^2} &= 0, \quad x_0 < x < x_1, \\
\frac{EI_2}{L^4} \frac{\partial y_2^4(x, t)}{\partial x^4} + \rho A_2 \frac{\partial^2 y_2(x, t)}{\partial t^2} &= 0, \quad x_1 < x < x_2,
\end{aligned}$$

$$\begin{aligned}
\frac{EI_3}{L^4} \frac{\partial y_3^4(x, t)}{\partial x^4} + \rho A_3 \frac{\partial^2 y_3(x, t)}{\partial t^2} &= 0, \quad x_1 < x < x_2, \\
\frac{EI_4}{L^4} \frac{\partial y_4^4(x, t)}{\partial x^4} + \rho A_4 \frac{\partial^2 y_4(x, t)}{\partial t^2} &= 0, \quad x_2 < x < x_3.
\end{aligned} \quad (21)$$

The matching conditions in Eqs. (18) and (19) become

$$\begin{aligned}
y_1(x_1^-, t) &= y_2(x_1^+, t), \quad y_1(x_1^-, t) = y_3(x_1^+, t), \\
y_4(x_2^+, t) &= y_2(x_2^-, t), \quad y_4(x_2^+, t) = y_3(x_2^-, t), \\
y_1'''(x_1^-, t) &= h_c^3 y_2'''(x_1^+, t) + (1 - h_c)^3 y_3'''(x_1^+, t), \\
y_1''''(x_1^-, t) &= h_c^3 y_2''''(x_1^+, t) + (1 - h_c)^3 y_3''''(x_1^+, t), \\
y_4''(x_2^+, t) &= h_c^3 y_2''(x_2^-, t) + (1 - h_c)^3 y_3''(x_2^-, t), \\
y_4''''(x_2^+, t) &= h_c^3 y_2''''(x_2^-, t) + (1 - h_c)^3 y_3''''(x_2^-, t), \\
y_2'(x_1^+, t) - y_1'(x_1^-, t) &= c_1 h_c^3 y_2''(x_1^+, t), \\
y_3'(x_1^+, t) - y_1'(x_1^-, t) &= c_2 (1 - h_c)^3 y_3''(x_1^+, t), \\
y_4'(x_2^+, t) - y_2'(x_2^-, t) &= c_3 h_c^3 y_2''(x_2^-, t), \\
y_4'(x_2^+, t) - y_3'(x_2^-, t) &= c_4 (1 - h_c)^3 y_3''(x_2^-, t).
\end{aligned} \quad (22)$$

Let $y_i(x, t) = w_i(x) \exp(j\omega t)$, where ω is a natural frequency of the four-beam model, and $w_i(x)$ is the corresponding mode shape of the i th beam segment; Eq. (21) becomes

$$\begin{aligned}
w_1''''(x) - \lambda_1^4 w_1(x) &= 0, \quad x_0 < x < x_1, \\
w_2''''(x) - \lambda_2^4 w_2(x) &= 0, \quad x_1 < x < x_2, \\
w_3''''(x) - \lambda_3^4 w_3(x) &= 0, \quad x_1 < x < x_2, \\
w_4''''(x) - \lambda_4^4 w_4(x) &= 0, \quad x_2 < x < x_3,
\end{aligned} \quad (23)$$

where

$$\begin{aligned}
\lambda_1^4 &= \frac{\rho A_1 \omega^2 L^4}{EI_1}, \quad \lambda_2^4 = \frac{\rho A_2 \omega^2 L^4}{EI_2}, \\
\lambda_3^4 &= \frac{\rho A_3 \omega^2 L^4}{EI_3}, \quad \lambda_4^4 = \frac{\rho A_4 \omega^2 L^4}{EI_4}.
\end{aligned} \quad (24)$$

The general solution of Eq. (23) for each beam segment is

$$\begin{aligned}
w_i(x) &= \bar{A}_i \sin \lambda_i (x - x_{i-1}) + \bar{B}_i \cos \lambda_i (x - x_{i-1}) + \\
&\quad \bar{C}_i \sinh \lambda_i (x - x_{i-1}) + \bar{D}_i \cosh \lambda_i (x - x_{i-1}), \quad (25) \\
&\quad x_{i-1} < x < x_i,
\end{aligned}$$

where \bar{A}_i , \bar{B}_i , \bar{C}_i , and \bar{D}_i are unknown constants associated with the i th beam segment. By Eq. (22), one can relate the unknown constants associated with the $(i+1)$ th ($i=1, 2, 3$) beam segment to those with the i th beam segment:

$$\mathbf{G}_1 \begin{pmatrix} \bar{A}_1 \\ \bar{B}_1 \\ \bar{C}_1 \\ \bar{D}_1 \end{pmatrix} = \mathbf{G}_2 \begin{pmatrix} \bar{A}_2 \\ \bar{B}_2 \\ \bar{C}_2 \\ \bar{A}_3 \\ \bar{B}_3 \\ \bar{C}_3 \\ \bar{D}_3 \end{pmatrix}, \quad (26)$$

$$\mathbf{G}_3 \begin{pmatrix} \bar{A}_2 \\ \bar{B}_2 \\ \bar{C}_2 \\ \bar{D}_2 \\ \bar{A}_3 \\ \bar{B}_3 \\ \bar{C}_3 \\ \bar{D}_3 \end{pmatrix} = \mathbf{G}_4 \begin{pmatrix} \bar{A}_4 \\ \bar{B}_4 \\ \bar{C}_4 \\ \bar{D}_4 \end{pmatrix}. \quad (27)$$

Where entries of matrices \mathbf{G}_1 , \mathbf{G}_2 , \mathbf{G}_3 , and \mathbf{G}_4 are given in Appendix B. By Eqs. (26) and (27), one has

$$\begin{pmatrix} \bar{A}_2 \\ \bar{B}_2 \\ \bar{C}_2 \\ \bar{D}_2 \\ \bar{A}_3 \\ \bar{B}_3 \\ \bar{C}_3 \\ \bar{D}_3 \end{pmatrix} = \mathbf{G}_2^{-1} \mathbf{G}_1 \begin{pmatrix} \bar{A}_1 \\ \bar{B}_1 \\ \bar{C}_1 \\ \bar{D}_1 \end{pmatrix}, \quad (28)$$

$$\begin{pmatrix} \bar{A}_4 \\ \bar{B}_4 \\ \bar{C}_4 \\ \bar{D}_4 \end{pmatrix} = \mathbf{G}_4^{-1} \mathbf{G}_3 \mathbf{G}_2^{-1} \mathbf{G}_1 \begin{pmatrix} \bar{A}_1 \\ \bar{B}_1 \\ \bar{C}_1 \\ \bar{D}_1 \end{pmatrix}. \quad (29)$$

The boundary conditions in Eq. (17) become

$$w(0) = 0, \quad w'(0) = 0, \quad (30)$$

$$w''(1) = 0, \quad w'''(1) = 0. \quad (31)$$

Applying the boundary conditions in Eq. (30) to Eq. (25) yields

$$\bar{A}_1 + \bar{C}_1 = 0, \quad \bar{B}_1 + \bar{D}_1 = 0. \quad (32)$$

Applying the boundary conditions in Eq. (31) to Eq. (25) yields

$$-\lambda_4^2 \bar{A}_4 \sin \lambda_4 l_4 - \lambda_4^2 \bar{B}_4 \cos \lambda_4 l_4 + \lambda_4^2 \bar{C}_4 \sinh \lambda_4 l_4 + \lambda_4^2 \bar{D}_4 \cosh \lambda_4 l_4 = 0, \quad (33)$$

$$-\lambda_4^3 \bar{A}_4 \cos \lambda_4 l_4 + \lambda_4^3 \bar{B}_4 \sin \lambda_4 l_4 + \lambda_4^3 \bar{C}_4 \cosh \lambda_4 l_4 + \lambda_4^3 \bar{D}_4 \sinh \lambda_4 l_4 = 0. \quad (34)$$

Eqs. (33) and (34) can be written in the matrix form

$$\mathbf{B} \begin{pmatrix} \bar{A}_4 \\ \bar{B}_4 \\ \bar{C}_4 \\ \bar{D}_4 \end{pmatrix} = \begin{pmatrix} 0 \\ 0 \end{pmatrix}, \quad (35)$$

where

$$\mathbf{B} = \begin{pmatrix} -\sin \lambda_4 l_4 & -\cos \lambda_4 l_4 & \sinh \lambda_4 l_4 & \cosh \lambda_4 l_4 \\ -\cos \lambda_4 l_4 & \sin \lambda_4 l_4 & \cosh \lambda_4 l_4 & \sinh \lambda_4 l_4 \end{pmatrix}. \quad (36)$$

Substituting Eq. (35) into Eq. (29) yields

$$\begin{pmatrix} 0 \\ 0 \end{pmatrix} = \mathbf{B} \begin{pmatrix} \bar{A}_4 \\ \bar{B}_4 \\ \bar{C}_4 \\ \bar{D}_4 \end{pmatrix} = \mathbf{B} \mathbf{G}_4^{-1} \mathbf{G}_3 \mathbf{G}_2^{-1} \mathbf{G}_1 \begin{pmatrix} \bar{A}_1 \\ \bar{B}_1 \\ \bar{C}_1 \\ \bar{D}_1 \end{pmatrix}. \quad (37)$$

Let

$$\mathbf{R} = \mathbf{B} \mathbf{G}_4^{-1} \mathbf{G}_3 \mathbf{G}_2^{-1} \mathbf{G}_1 = \begin{pmatrix} R_{11} & R_{12} & R_{13} & R_{14} \\ R_{21} & R_{22} & R_{23} & R_{24} \end{pmatrix}, \quad (38)$$

use of Eqs. (32), (37), and (38) yields

$$\begin{pmatrix} R_{11} - R_{13} & R_{12} - R_{14} \\ R_{21} - R_{23} & R_{22} - R_{24} \end{pmatrix} \begin{pmatrix} \bar{A}_1 \\ \bar{B}_1 \end{pmatrix} = \begin{pmatrix} 0 \\ 0 \end{pmatrix}. \quad (39)$$

Existence of a non-trivial solution of Eq. (39) requires

$$\det \begin{pmatrix} R_{11} - R_{13} & R_{12} - R_{14} \\ R_{21} - R_{23} & R_{22} - R_{24} \end{pmatrix} = 0, \quad (40)$$

which is the frequency equation of the four-beam model $f(\omega)=0$. The n th natural frequency of the four-beam model is the n th positive root of the frequency equation. By Eqs. (28), (29), (37), (39), and (40), and assuming \bar{B}_1 has an arbitrary known value, one can obtain all the other constants of \bar{A}_i , \bar{B}_i , \bar{C}_i , and \bar{D}_i in $w_i(x)$ in Eq. (25). The normalized n th mode shape of the four-beam model is defined by

$$\hat{w}_n(x) = \frac{w_n(x)}{\max(w_n(x))}. \quad (41)$$

3 Numerical Results

3.1 Comparison of natural frequencies and mode shapes of the four-beam model and a FE model

Consider a cantilever beam with $L=600$ mm, $h=b=10$ mm, $E=206$ GN/m², $\nu=0.3$, and $\rho=7800$ kg/m³. Numerical results of natural frequencies and mode shapes of the four-beam model are compared with those from commercial FE software^[45], 2D singular elements PLANE183, which are six-node shell elements with two

degrees of freedom at each node, are used around the crack tips of the cantilever beam in the FE model. The other parts of the beam are meshed by 2D solid elements PLANE 42. Contact between nodes in the crack region is ignored in the FE model. Table 1 shows the first three natural frequencies of the four-beam model and the FE model. It is shown that the first three natural frequencies of the undamaged beam from the proposed model, which are the same as those of the uniform cantilever beam, are close to those of the FE model, and their differences range from 0.13% to 0.26%. For cracked cantilever beams, the differences between the first three natural frequencies of the four-beam model and the FE model range from 3.79% to 31.20%, and the natural frequencies decrease with the crack length and depth. In the proposed model, an undamaged beam has three undamaged beam segments. The top beam segment is considered as a beam segment with a zero height. The other three beam segments are assumed to be Euler-Bernoulli beams.

Table 1. Comparison between the first three natural frequencies of the four-beam model and the FE model

Model	$X_1/L \times h_1/h$	L_2/L	Natural frequency/Hz		
			ω_1	ω_2	ω_3
Four-beam model	0×0	0	23.060	144.516	404.649
FE model			23.089	144.443	403.590
Difference/%			0.126	0.051	0.262
Four-beam model	0.25×0.4	0.1	19.465	138.258	353.332
FE model			23.059	143.637	403.532
Difference/%			-15.481	-3.794	-12.669
Four-beam model	0.25×0.4	0.15	18.088	130.762	344.849
FE model			23.036	142.463	403.363
Difference/%			-21.381	-8.260	-14.730
Four-beam model	0.2×0.2	0.2	19.465	135.218	361.242
FE model			23.033	142.294	400.106
Difference/%			-15.386	-5.021	-9.950
Four-beam model	0.2×0.3	0.2	17.563	130.849	350.189
FE model			22.991	140.644	400.648
Difference/%			-23.514	-7.011	-12.823
Four-beam model	0.3×0.4	0.2	17.435	112.960	335.650
FE model			22.995	142.505	385.079
Difference/%			-24.082	-20.772	-13.064
Four-beam model	0.4×0.4	0.2	18.852	99.400	319.766
FE model			22.991	144.408	368.310
Difference/%			-17.900	-31.202	-13.407

Fig. 4 shows the first three normalized mode shapes of beam segments 1, 2, and 4 of the four-beam model and those of the FE model; the amplitudes of beam segment 3 are almost the same as those of beam segment 2 for the four-beam model and the FE model. Fig. 4(a) shows that the normalized mode shapes of the undamaged beam from the proposed model, which are the same as those of the

uniform cantilever beam, are in excellent agreement with those of the FE model. Fig. 4(b) shows that the normalized mode shapes of the cracked cantilever beam with $X_1/L=0.25$, $h_1/h=0.5$, and $L_2/L=0.15$ from the proposed model are similar to those of the FE model.

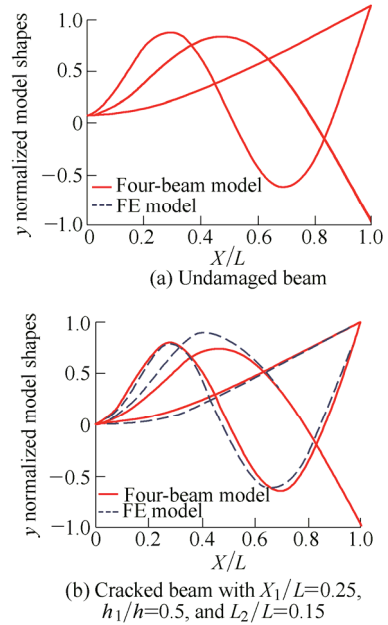


Fig. 4. First three normalized mode shapes of the four-beam model and the FE model

The modal assurance criterion(MAC) values are used to evaluate the differences between the mode shapes of the four-beam model and the FE model; they are defined by^[46]

$$M_A(U, V) = \frac{\left| \sum_{j=1}^n (\psi_U)_j (\psi_V)_j^* \right|^2}{\left[\sum_{j=1}^n (\psi_U)_j (\psi_U)_j^* \right] \left[\sum_{j=1}^n (\psi_V)_j (\psi_V)_j^* \right]}, \quad (42)$$

where the superscript * denotes complex conjugation, ψ_U is a mode shape of the four-beam model, ψ_V is a mode shape of the FE model or an experimentally measured mode shape, and n is the number of degrees of freedom for which ψ_U and ψ_V are available. Table 2 shows the MAC values between the first three mode shapes of the undamaged beam from the proposed model and those of the FE model, where $n=601$; the diagonal entries of the MAC matrix are one and the off-diagonal entries are almost zero, which means that the first three mode shapes of the undamaged beam are almost the same as those of the FE model. Table 3 shows the MAC values between the first three mode shapes of the cracked cantilever beam with $X_1/L=0.25$, $h_1/h=0.5$, and $L_2/L=0.15$ from the proposed model and those of the FE model, where $n=601$; the diagonal entries of the MAC matrix range from 0.980 to 0.998, and the off-diagonal entries range from 0.001 to 0.011.

Table 2. MAC values between first three mode shapes of undamaged beam from the proposed model and the FE model

Method		Four-beam model		
		1st mode	2nd mode	3rd mode
FE model	1st mode	1.000	1.159×10^{-5}	1.105×10^{-5}
	2nd mode	9.273×10^{-6}	1.000	1.094×10^{-5}
	3rd mode	9.820×10^{-6}	7.925×10^{-6}	1.000

Table 3. MAC values between first three mode shapes of cracked cantilever beam from the proposed model and the FE model

Method		Four-beam model		
		1st mode	2nd mode	3rd mode
FE model	1st mode	0.998	0.002	0.001
	2nd mode	0.002	0.988	0.011
	3rd mode	0.001	0.009	0.980

3.2 Effects of crack length, depth, and location on natural frequencies

Fig. 5 shows the effects of the crack length(L_2/L) and

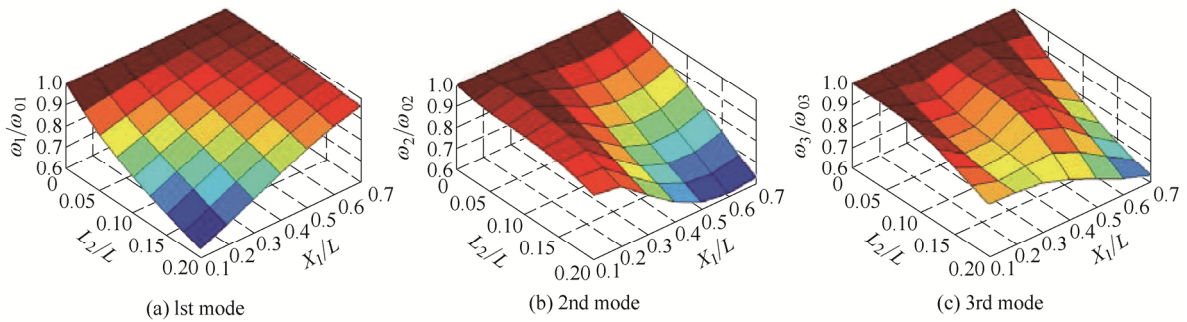


Fig. 5. Effects of crack length(L_2/L) and location(X_1/L) on natural frequency ratios of the cracked cantilever beam with $h_1/h=0.4$

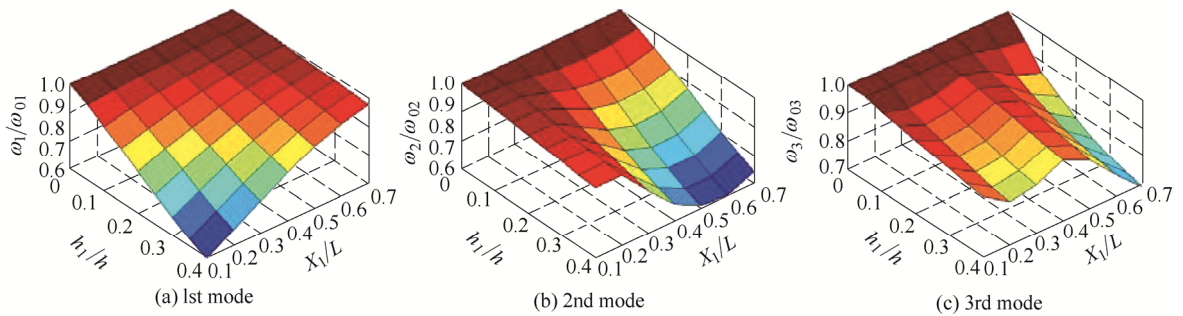


Fig. 6. Effects of crack depth(h_1/h) and location(X_1/L) on natural frequency ratios of the cracked cantilever beam with $L_2/L=0.15$

3.3 Effects of crack length, depth, and location on mode shapes

The effects of the crack length, depth, and location on CWT coefficients with a scale of 20 of the first three normalized mode shapes of the cracked cantilever beam are shown in Figs. 7–9, respectively.

The crack lengths and locations can be clearly and directly identified from sudden changes in spatial variations of the wavelet coefficients of the first three normalized mode shapes of the cracked cantilever beam, where the cracks are located between lines a and b, lines a and c, and lines a and d in Fig. 7; between lines a and b in Fig. 8; and

location(X_1/L) on the first three natural frequency ratios ω_n/ω_{0n} , where ω_n and ω_{0n} are the natural frequencies of the cracked cantilever beam with $h_1/h=0.4$ and the undamaged beam, respectively, calculated from the four-beam model. The first three natural frequencies of the cracked cantilever beam decrease with the increase of the crack length because the stiffness of the beam decreases with the increase of the crack length. The natural frequencies of the cracked cantilever beam are significantly affected by the crack location. The first natural frequency is more sensitive to a crack near the fixed end of the beam, and the second and third natural frequencies are more sensitive to a crack near the free end of the beam. Fig. 6 shows the effects of the crack depth(h_1/h) and location(X_1/L) on the first three natural frequency ratios of the cracked beam with $L_2/L=0.15$, calculated from the four-beam model. The first three frequencies decrease with the increase of the crack depth.

between lines a and d, lines b and e, and lines c and f in Fig. 9.

In Fig. 7, case 1 denotes the beam without a crack; case 2 denotes beam segments 1, 2, and 4 with $X_1/L=0.5$, $L_2/L=0.1$, and $h_1/h=0.4$; case 3 denotes beam segments 1, 3, and 4 with $X_1/L=0.5$, $L_2/L=0.1$, and $h_1/h=0.4$; case 4 denotes beam segments 1, 2, and 4 with $X_1/L=0.5$, $L_2/L=0.15$, and $h_1/h=0.4$; case 5 denotes beam segments 1, 3, and 4 with $X_1/L=0.5$, $L_2/L=0.15$, and $h_1/h=0.4$; case 6 denotes beam segments 1, 2, and 4 with $X_1/L=0.5$, $L_2/L=0.2$, and $h_1/h=0.4$; and case 7 denotes beam segments 1, 3, and 4 with $X_1/L=0.5$, $L_2/L=0.2$, and $h_1/h=0.4$.

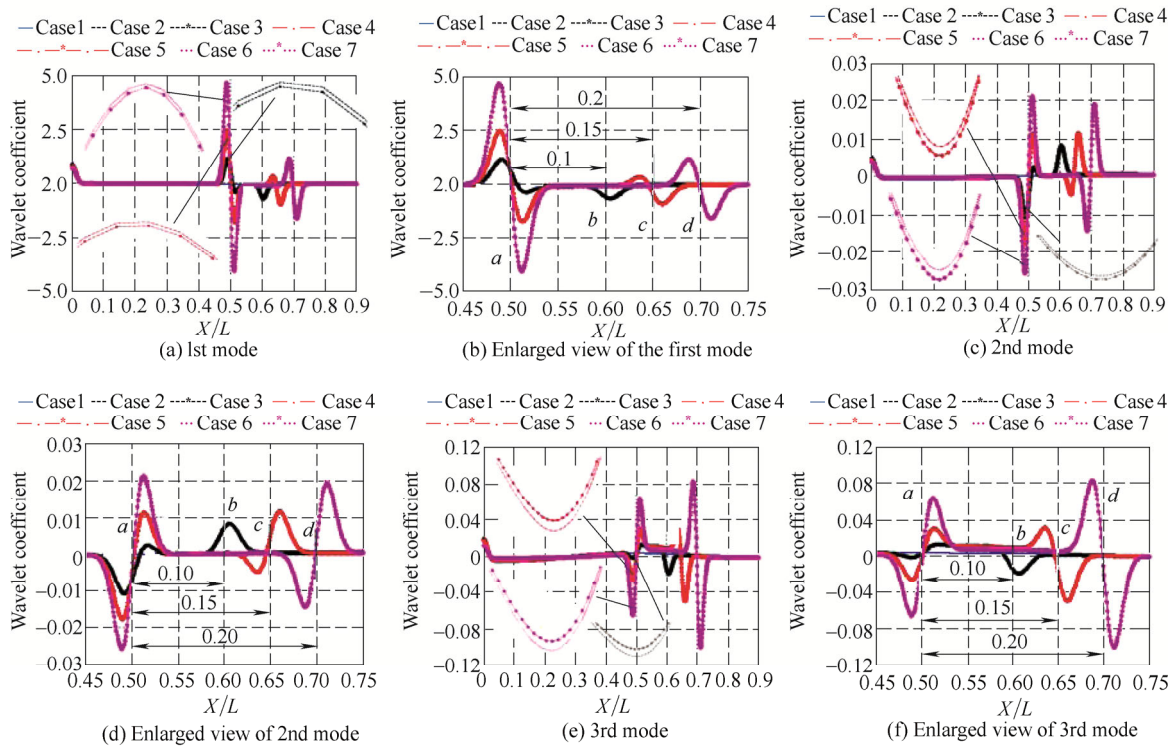


Fig. 7. Effect of crack length on wavelet coefficients of first three normalized mode shapes of the beam with and without a crack

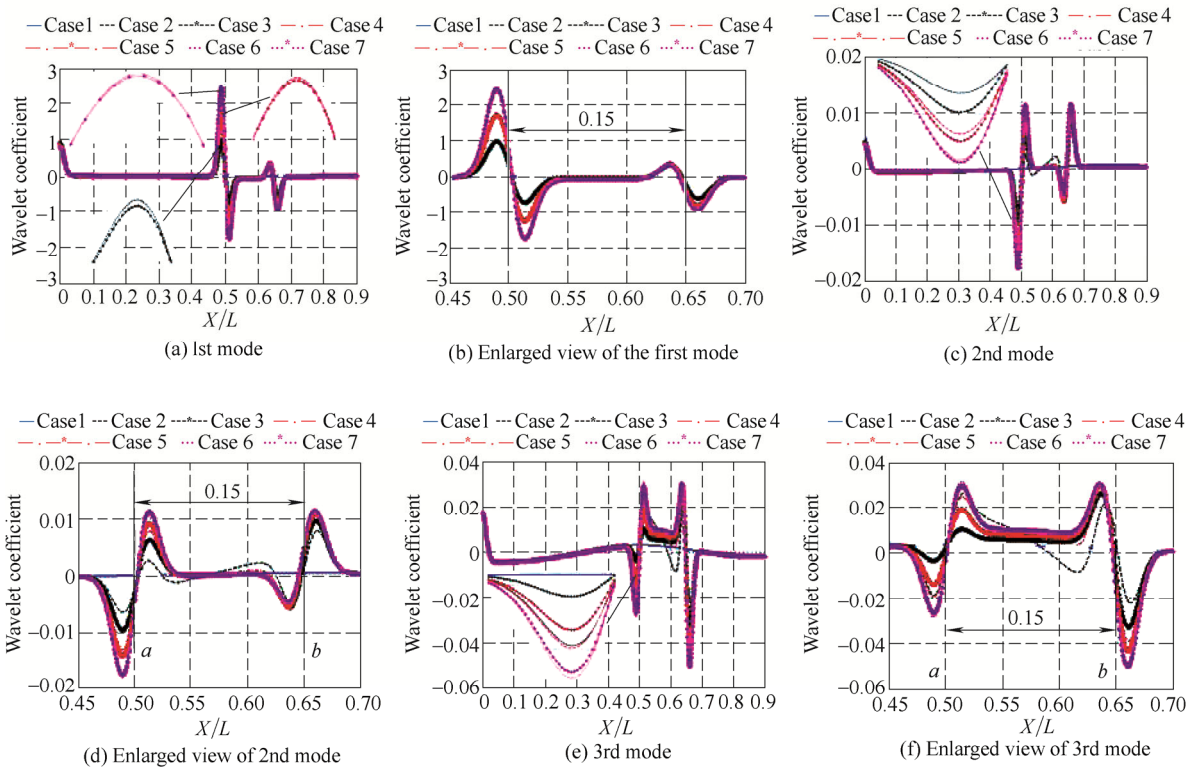


Fig. 8. Effect of crack depth on wavelet coefficients of first three normalized mode shapes of the beam with and without the crack

In Fig. 8, case 1 denotes the beam without a crack; case 2 denotes beam segments 1, 2, and 4 with $X_1/L=0.5$, $L_2/L=0.15$, and $h_1/h=0.2$; case 3 denotes beam segments 1, 3, and 4 with $X_1/L=0.5$, $L_2/L=0.15$, and $h_1/h=0.2$; case 4 denotes beam segments 1, 2, and 4, $X_1/L=0.5$, $L_2/L=0.15$, and $h_1/h=0.3$; case 5 denotes beam segments 1, 3, and 4 with $X_1/L=0.5$, $L_2/L=0.15$, and $h_1/h=0.3$; case 6 denotes beam segments 1, 2, and 4 with $X_1/L=0.5$, $L_2/L=0.15$, and

$h_1/h=0.4$; case 7 denotes beam segments 1, 3, and 4 with $X_1/L=0.5$, $L_2/L=0.15$, and $h_1/h=0.4$.

In Fig. 9, case 1 denotes the beam without a crack; case 2 denotes beam segments 1, 2, and 4 with $X_1/L=0.4$, $L_2/L=0.15$, and $h_1/h=0.4$; case 3 denotes beam segments 1, 3, and 4 with $X_1/L=0.4$, $L_2/L=0.15$, and $h_1/h=0.4$; case 4 denotes beam segments 1, 2, and 4 with $X_1/L=0.5$, $L_2/L=0.15$, and $h_1/h=0.4$; case 5 denotes beam segments 1,

3, and 4 with $X_1/L=0.5$, $L_2/L=0.15$, and $h_1/h=0.4$; case 6 denotes beam segments 1, 2, and 4 with $X_1/L=0.6$, $L_2/L=0.15$, and $h_1/h=0.4$; case 7 denotes beam segments 1, 3, and 4, $X_1/L=0.6$, $L_2/L=0.15$, and $h_1/h=0.4$.

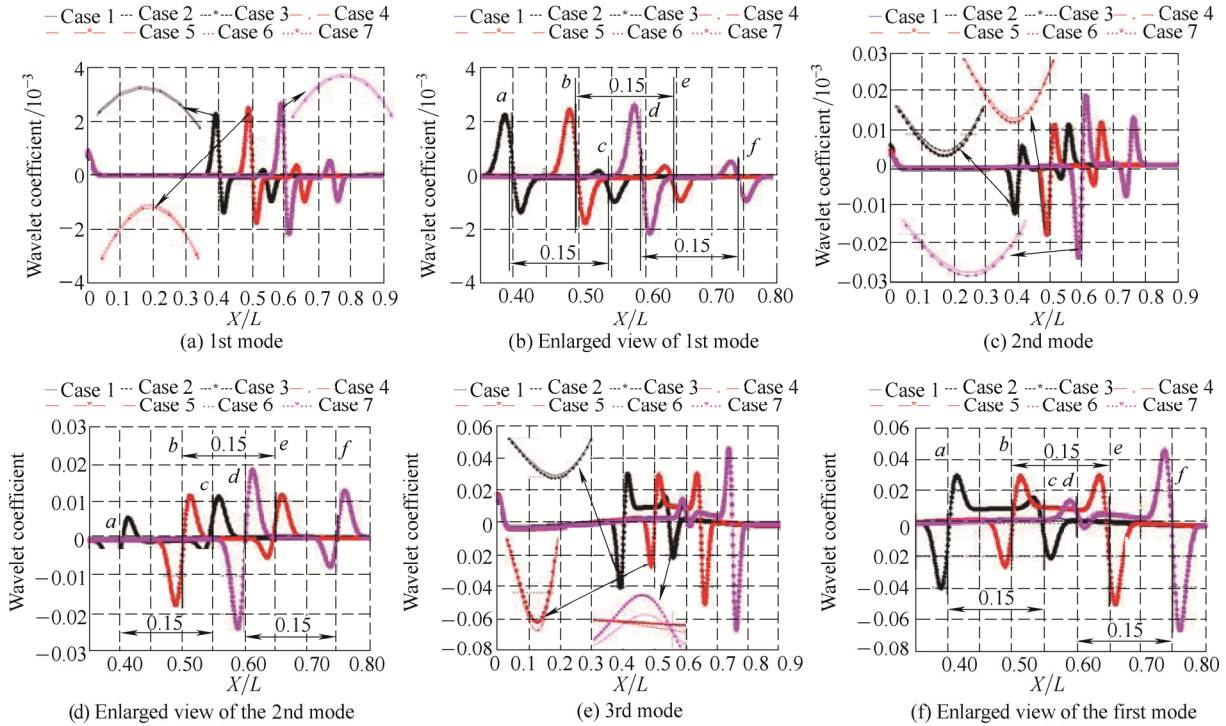


Fig. 9. Effect of crack location on wavelet coefficients of first three normalized mode shapes of the beam with and without the crack

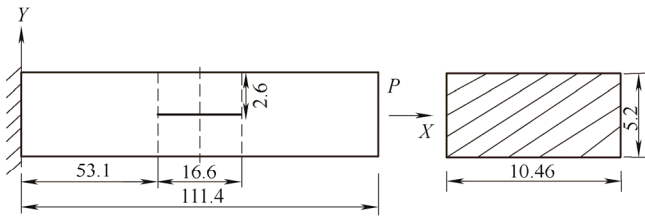
Note that lines a through f are located at the centers of the sudden changes that look like sine waves, and the crack tips are not located at the peaks of the sine waves. The periods of these sine waves are about $0.1L$, which are slightly affected by the crack length, depth, and location. As shown in Fig. 8, the amplitudes of the sudden changes in the spatial variations of the wavelet coefficients of the first and third normalized mode shapes of beam segments 1, 2, and 4 are larger than those of beam segments 1, 3, and 4. The amplitudes of the sudden changes in the spatial variations of the wavelet coefficients of the second mode shape of beam segments 1, 2, and 4 are smaller than those of beam segments 1, 3, and 4. Similar results are observed in Figs. 8 and 9. It can be seen from Figs. 7 and 8 that the amplitudes of the sudden changes in the spatial variations of the wavelet coefficients increase with the crack length and depth. It can also be seen from Fig. 9 that the amplitudes of the sudden changes in the spatial variations of the wavelet coefficients become larger when the crack gets closer to the free end of the beam.

4 Experimental Validation

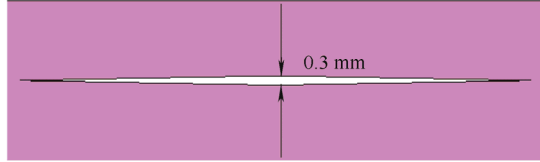
To validate the four-beam model, the first three natural frequencies and mode shapes of a cantilever beam with an embedded horizontal crack are measured. The cracked beam is made of acrylonitrile butadiene styrene using a 3D printer. The length, width, and thickness of the beam are 111.4 mm, 10.5 mm, and 5.2 mm, respectively, and the

length, width, and height of the crack are 16.6 mm, 10.5 mm, and 0.3 mm, respectively, as shown in Figs. 10(a) and (b). The distance between the left end of the crack and the fixed end of the beam is 53.1 mm, and that between the top surface of the crack and the top surface of the beam is 2.6 mm.

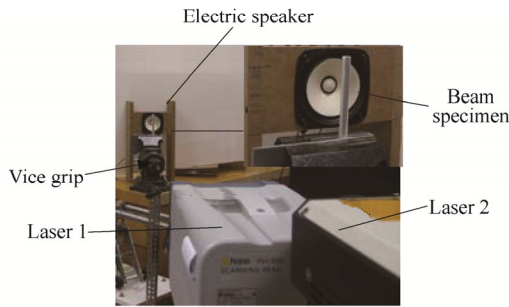
In order to get precise natural frequency and mode shape measurement without incurring mass loading, an operational modal analysis(OMA) with non-contact excitation and measurement^[47] is performed, and an experimental setup is shown in Fig. 10(c). To create a fixed boundary of the cantilever beam, a vice grip is used to firmly clamp two flat metal plates, and the fixed end of the beam is clamped between the two plates. An electric speaker with a wooden fixture faces the beam and generates acoustic excitation to it. Two Doppler laser vibrometers are used to measure the responses of the beam: Laser 1 in Fig. 10(c) is a Polytec PSV-500 scanning laser vibrometer that measures velocities of measurement points on the beam, and Laser 2 is a Polytec OFV-353 single-point laser vibrometer that measures the velocity of a reference point on the beam. There are totally 129 measurement points on the beam, which are evenly distributed along the length of the beam. Acoustic excitation in the form of burst chirp is used to excite the beam, and cross power spectral densities between the velocities of the measurement points and that of the reference point are calculated, from which the first three natural frequencies and mode shapes of the beam are calculated by Operational PolyMax of LMS Test. Lab Rev. 9b.



(a) Dimensions of a cantilever beam with an embedded crack(mm)



(b) Enlarged view of the crack region



(c) Experimental setup using OMA

Fig. 10. Experimental setup

The FE model of the test beam is constructed using commercial FE software^[45]. The material properties of beam are $E=2.10 \times 10^9$ N/m², $\nu=0.4$, and $\rho=1000$ kg/m³. Table 1 shows the first three natural frequencies from the experiment, the FE model, and the four-beam model, and the differences between the measured and calculated natural frequencies. The differences between the first three natural frequencies from the FE model and the experiment are -0.67% , -0.63% , and -0.25% , respectively. The first three natural frequencies of the test beam from the FE model are in excellent agreement with those from the experiment. The differences between the first three natural frequencies from the four-beam model and the experiment are -8.84% , -29.88% , and -4.49% , respectively. While the differences between the first and third natural frequencies from the four-beam model and the experiment are small, the difference between the second natural frequency from the four-beam model and the experiment is relatively large because there is a turning point of the second mode shape

near the center of the crack(see Fig. 11(b)). The differences between the first three natural frequencies from the four-beam model and the experiment may also be caused by the fact that there is no gap in the crack region in the four-beam model and there is a gap in the crack region of the test beam.

Table 4. Comparison among first three natural frequencies of the test beam from the experiment, the FE model, and the four-beam model

Method	Natural frequencies ω /Hz		
	1st mode	2nd mode	3rd mode
Experiment	97.14	615.00	1608.00
FE model	97.79	611.10	1604.00
Difference/%	0.67	-0.63	-0.25
Four-beam model	88.55	431.26	1535.85
Difference /%	-8.84	-29.88	-4.49

Fig. 11 shows the first three normalized mode shapes of beam segments 1, 2, and 4 from the experiment, the FE model, and the four-beam model, where the mode shapes from the experiment are real parts of the mode shapes. Table 5 shows the MAC values between the first three normalized mode shapes of the test beam from the experiment and the FE model; the diagonal entries of the MAC matrix range from 0.935 to 1.000, and the off-diagonal entries range from 0.000 2 to 0.015. Table 6 shows the MAC values between the first three normalized mode shapes of the test beam from the experiment and the four-beam model; the diagonal entries of the MAC matrix range from 0.919 to 0.993, and the off-diagonal entries range from 0 to 0.036. Table 7 shows the MAC values between the first three normalized mode shapes of the test beam from the four-beam model and the FE model; the diagonal entries of the MAC matrix range from 0.984 to 0.994, and the off-diagonal entries range from 0.000 1 to 0.007. The first three normalized mode shapes of the test beam from the experiment agree very well with those from the FE model, and they are similar to those from the four-beam model. The wavelet coefficients of the third normalized mode shape from the experiment, the FE model, and the four-beam model are also compared, as shown in Fig. 12. Sudden changes in the spatial variations of the wavelet coefficients are observed in the crack region from the three different methods; the waveforms of the sudden changes are similar. The results from the experiment and the FE model validate those from the four-beam model.

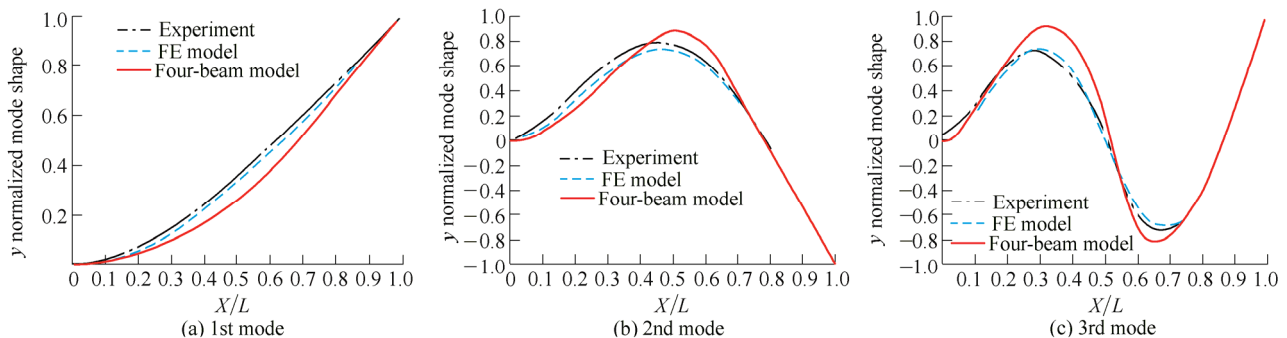


Fig. 11. First three normalized mode shapes from the experiment, the FE model, and the four-beam model

Table 5. MAC values between first three mode shapes of the test beam from the experiment and the FE model($n=129$)

Method	FE model			
	1st mode	2nd mode	3rd mode	
Experiment	1st mode	1.000 0	0.000 0	0.000 3
	2nd mode	0.000 3	0.997 0	0.000 7
	3rd mode	0.040 0	0.015 0	0.935 0

Table 6. MAC values between first three mode shapes of test beam from the experiment and the four-beam model($n=129$)

Method	Four-beam model			
	1st mode	2nd mode	3rd mode	
Experiment	1st mode	0.993 0	0.005 0	0.000 2
	2nd mode	0.003 0	0.976 0	0.010 0
	3rd mode	0.036 0	0.032 0	0.919 0

Table 7. MAC values between first three mode shapes of the test beam from the four-beam model and the FE model($n=129$)

Method	Four-beam model			
	1st mode	2nd mode	3rd mode	
FE model	1st mode	0.994 0	0.004 0	0.000 1
	2nd mode	0.007 0	0.984 0	0.004 0
	3rd mode	0.005 0	0.007 0	0.989 0

5 Conclusions

(1) A new four-beam model with local flexibilities at crack tips is developed. Two separate beam segments are used to model the crack region so that the crack can be open. The governing equations and the matching and boundary conditions of the four-beam model are derived using Hamilton’s principle.

(2) The compliance between beam segments 1 and 2 is more than that between beam segments 2 and 4. The compliance between beam segments 1 and 3 is more than that between beam segments 3 and 4. All the compliances increase with the crack length and depth.

(3) For the undamaged cantilever beam, the differences between the first three natural frequencies from the proposed model and those of the FE model range from 0.05% to 0.26%; the diagonal entries of the MAC matrix between the corresponding mode shapes are one and its off-diagonal entries are almost zero. For a cracked cantilever beam, the

differences between the first three natural frequencies of the four-beam model and those of the FE model range from 3.79% to 31.20%; the diagonal and off-diagonal entries of the MAC matrix between the corresponding mode shapes range from 0.980 to 0.998 and from 0.001 to 0.011, respectively.

(4) The first three natural frequencies of the cracked cantilever beam decrease with the increase of the crack length and depth. They can also be significantly affected by the crack location. The first natural frequency is more sensitive to a crack near the fixed end of the beam, and the second and third natural frequencies are more sensitive to a crack near the free end of the beam.

(5) The amplitudes of the sudden changes in the spatial variations of CWT coefficients of the first three normalized mode shapes increase with the crack length and depth, and the distance between the crack center and the fixed end of the cracked cantilever beam. The amplitudes of the sudden changes in the spatial variations of the wavelet coefficients of the first and third normalized mode shapes of beam segments 1, 2, and 4 are larger than those of beam segments 1, 3, and 4; the amplitudes of the sudden changes in the spatial variations of the wavelet coefficients of the second normalized mode shape of beam segments 1, 2, and 4 are smaller than those of beam segments 1, 3, and 4. The CWT method can be used to identify the crack length and location.

(6) The sudden changes in the spatial variations of the wavelet coefficients look like sine waves, and the crack tips are located at the centers of the sine waves. The periods of the sine waves are about $0.1L$, which are slightly affected by the crack length, depth, and location.

(7) The differences between the first three natural frequencies of the test beam from the FE model and the experiment are $-0.67%$, $-0.63%$, and $-0.25%$, respectively. The first three natural frequencies of the test beam from the FE model are in excellent agreement with those from the experiment. The differences between the first three natural frequencies from the four-beam model and the experiment are $-8.84%$, $-29.88%$, and $-4.49%$, respectively. Sudden changes in the spatial variations of the wavelet coefficients are observed in the crack region from the experiment, the FE model, and the four-beam model; the waveforms of the sudden changes are also similar.

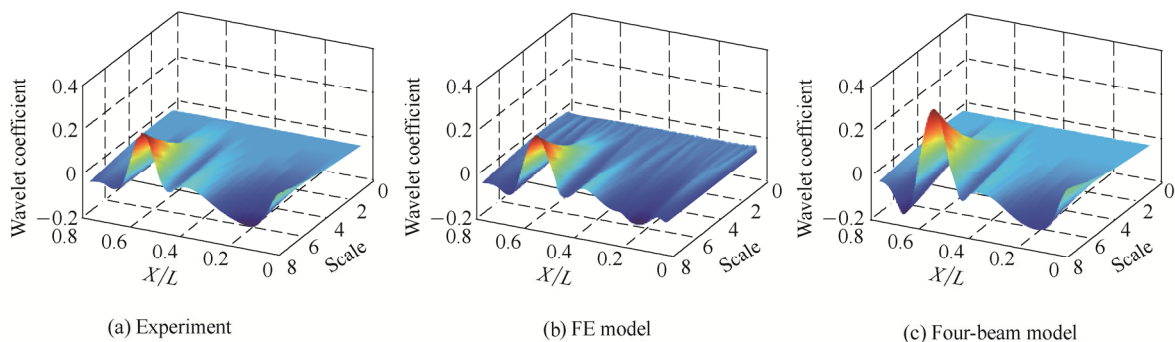


Fig. 12. Comparison among the wavelet coefficients of the third normalized mode shape from different methods

References

- [1] FAN W, QIAO P Z. Vibration-based damage identification methods: a review and comparative study[J]. *Structural Health Monitoring*, 2011, 10(1): 83–111.
- [2] JASSIM Z A, ALI N N, MUSTAPHA F, et al. A review on the vibration analysis for a damage occurrence of a cantilever beam[J]. *Engineering Failure Analysis*, 2013, 31(1): 442–461.
- [3] OSTACHOWICZ W M, KRAWCZUK M. Analysis of the effect of cracks on the natural frequencies of a cantilever beam[J]. *Journal of Sound and Vibration*, 1991, 150(2): 191–201.
- [4] WANG K H, INMAN D J, FARRAR C R. Modeling and analysis of a cracked composite cantilever beam vibrating in coupled bending and torsion[J]. *Journal of Sound and Vibration*, 2005, 284(1): 23–49.
- [5] BOVSUNOVSKY A P, MATVEEV V V. Analytical approach to the determination of dynamic characteristics of a beam with a closing crack[J]. *Journal of Sound and Vibration*, 2000, 235(3): 415–434.
- [6] YUEN M F. A numerical study of the eigenparameters of a damaged cantilever[J]. *Journal of Sound and Vibration*, 1985, 103(1): 301–310.
- [7] RIZOS P F, ASPRAGATHOS N. Identification of crack location and magnitude in a cantilever beam from the vibrating mode[J]. *Journal of Sound and Vibration*, 1990, 138(3): 381–388.
- [8] NANDWANA B P, MAITI S K. Detection of the location and size of a crack in stepped cantilever beams based on measurements of natural frequencies[J]. *Journal of Sound and Vibration*, 1997, 203(3): 435–446.
- [9] KISA M. Free vibration analysis of a cantilever composite beam with multiple cracks[J]. *Composites Science and Technology*, 2004, 64(9): 1391–1402.
- [10] NAHVI H, JABBARI M. Crack detection in beams using experimental modal data and finite element model[J]. *International Journal of Mechanical Sciences*, 2005, 47(1): 1477–1497.
- [11] LIN H P, CHANG S C. Forced response of cracked cantilever beams subjected to a concentrated moving load[J]. *International Journal of Mechanical Sciences*, 2006, 48(1): 1456–1463.
- [12] YANG J, CHEN Y. Free vibration and buckling analyses of functionally graded beams with edge cracks[J]. *Composite Structures*, 2008, 83(1): 48–60.
- [13] SEYEDPOOR S M. A two stage method for structural damage detection using a modal strain energy based index and particle swarm optimization[J]. *International Journal of Non-Linear Mechanics*, 2012, 47(1): 1–8.
- [14] LU X B, LIU J K, LU Z R. A two-step approach for crack identification in beam[J]. *Journal of Sound and Vibration*, 2013, 332(1): 282–293.
- [15] SHIFRIN E I, RUOTOLO R. Natural frequencies of a beam with an arbitrary number of cracks[J]. *Journal of Sound and Vibration*, 1999, 222(3): 409–423.
- [16] LIN H P, CHANG S C, WU J D. Beam vibrations with arbitrary number of cracks[J]. *Journal of Sound and Vibration*, 2002, 258(5): 987–999.
- [17] KHIEM N T, LIEN T V. Multi-crack detection for beam by the natural frequencies[J]. *Journal of Sound and Vibration*, 2004, 273(1): 175–184.
- [18] CHANG C C, CHEN L W. Detection of the location and size of cracks in the multiple cracked beam by spatial wavelet based approach[J]. *Mechanical Systems and Signal Processing*, 2005, 19(1): 139–155.
- [19] PATIL D P, MAITI S K. Experimental Verification of a method of detection of multiple cracks in beams based on frequency measurements[J]. *Journal of Sound and Vibration*, 2005, 281(1): 439–451.
- [20] MORADI S, KARGOZARFARD M. On multiple crack detection in beam structures[J]. *Journal of Mechanical Science and Technology*, 2013, 27(1): 47–55.
- [21] ZOU Y, TONG L, STEVEN G P. Vibration-based model-dependent damage(delamination) identification and health monitoring for composite structures—a review[J]. *Journal of Sound and Vibration*, 2000, 230(2): 357–378.
- [22] LEE J, HAFTKA R T, GRIFFIN O H. Detecting delaminations in a Composite beam using anti-optimization[J]. *Structural Optimization*, 1994, 8(2–3): 93–100.
- [23] MAJUMDAR P M, SURYANARAYAN S. Flexural vibrations of beams with delaminations[J]. *Journal of Sound and Vibration*, 1988, 125(3): 441–461.
- [24] TRACY J J, PARDOEN G C. Effect of delamination on the natural frequencies of composite laminates[J]. *Journal of Composite Materials*, 1989, 23(12): 1200–1215.
- [25] ISHAK S I, LIU G R, SHANG H M, et al. Non-destructive evaluation of horizontal crack detection in beams using transverse impact[J]. *Journal of Sound and Vibration*, 2002, 252(2): 343–360.
- [26] WILDY S J, KOTOUSOV A G, CAZZOLATO B S, et al. New damage detection technique based on governing differential equations of continuum mechanics. part I: out-of-plane loading[C]//*Proceedings of the 6th Australasian Congress on Applied Mechanics(ACAM 6)*, Perth, Australia, 2010.
- [27] QIAN X D, CAO M S, SU Z Q. A hybrid particle swarm optimization(PSO)—simplex algorithm for damage identification of delaminated beams[J]. *Mathematical Problems in Engineering*, 2012, 2012(1): 1–11.
- [28] LUO H, HANAGUD S. Dynamics of delaminated beams[J]. *International Journal of Solids and Structures*, 2000, 37: 1501–1519.
- [29] LEE J H. Free vibration analysis of delaminated composite beams[J]. *Computers and Structures*, 2000, 74(1): 121–129.
- [30] WU N, WANG Q. Repair of vibrating delaminated beam structures using piezoelectric patches[J]. *Smart Materials and Structures*, 2010, 19(1): 035027.
- [31] QIAO P Z, CHEN F L. On the improved dynamic analysis of delaminated beams[J]. *Journal of Sound and Vibration*, 2012, 331(1): 1143–1163.
- [32] WANG J, QIAO P Z. Novel beam analysis of end notched flexure specimen for mode — II fracture[J]. *Engineering Fracture Mechanics*, 2004, 71(1): 219–231.
- [33] LI B, CHEN X F, HE Z J. I-beam crack identification based on study of local flexibility due to crack[J]. *Chinese Journal of Mechanical Engineering*, 2013, 24(6): 1116–1122.
- [34] LI B, CHEN X F, HE Z J. Three-steps-meshing based multiple crack identification for structures and its experimental studies[J]. *Chinese Journal of Mechanical Engineering*, 2013, 26(2): 400–405.
- [35] YAZDI A K, SHOOSHTARI A. A new two-dimensional cracked finite element for fracture mechanics[J]. *Engineering Fracture Mechanics*, 2015, 135(1): 17–33.
- [36] CHU P, LI X F, WANG Z G, et al. Double cantilever beam model for functionally graded materials based on two-dimensional theory of elasticity[J]. *Engineering Fracture Mechanics*, 2015, 135(1): 232–244.
- [37] NANDAKUMAR P, SHANKAR K. Structural crack damage detection using transfer matrix and state vector[J]. *Measurement*, 2015, 68(1): 310–327.
- [38] FANG X. The mechanics of an elastically deforming cantilever beam with an embedded sharp crack and subjected to an end transverse loading[D]. *University of Maryland, Baltimore County, USA*, 2013.
- [39] DOUKAE, LOUSTRIDIS S, TROCHIDIS A. Crack identification in beams using wavelet analysis[J]. *International Journal of Solids and Structures*, 2003, 40(1): 3557–3569.
- [40] ORHAN S. Analysis of free and forced vibration of a cracked cantilever beam[J]. *NDT&E International*, 2007, 40(1): 443–450.
- [41] MASOUD A A, SAID S A. A new algorithm for crack location in a rotating Timoshenko beam[J]. *Journal of Vibration and Control*, 2009, 15(10): 1541–1561.

- [42] CAO M, YE L, ZHOU L. Sensitivity of fundamental mode shape and static deflection for damage identification in cantilever beams[J]. *Mechanical Systems and Signal Processing*, 2011, 25(2): 630–643.
- [43] LEE J. Identification of multiple cracks in a beam using vibration amplitude[J]. *Journal Sound and Vibration*, 2009, 326(1–2): 205–212.
- [44] KIM D G, LEE S B. Structural damage identification of a cantilever beam using excitation force level control[J]. *Mechanical Systems and Signal Processing*, 2010, 24(6): 1814–1830.
- [45] ANSYS *Theory Reference*[M]. ANSYS Release 11.0. ANSYS, Inc., 2007.
- [46] EWINS D J. *Modal Testing: Theory, practice and application*[M]. 2nd ed. Hertfordshire: Research Studies Press Ltd., 2000.
- [47] XU Y F, ZHU W D. Operational modal analysis of a rectangular plate using non-contact excitation and measurement[J]. *Journal of Sound and Vibration*, 2013, 332(20): 4927–4939.

Biographical notes

LIU Jing, born in 1983, is currently a lecturer at *State Key Laboratory of Mechanical Transmission, College of Mechanical Engineering, Chongqing University, China*. He received his PhD degree from *Chongqing University, China*, in 2014. His research interests include vibration, dynamics, and numerical modeling.
E-mail: jliu@cqu.edu.cn

ZHU Weidong, born in 1964, is a full professor at *Department of Mechanical Engineering, University of Maryland, Baltimore County, USA*. His research interests include dynamics, vibration, control, applied mechanics, structural health monitoring, and wind energy; his research integrates analytical development, numerical simulation, experimental validation, and industrial application.
E-mail: wzhu@umbc.edu

CHARALAMBIDES Panos G, born in 1955, is a full professor at *Department of Mechanical Engineering, University of Maryland, Baltimore County, USA*. His research interests include mechanics of materials and micromechanics modeling, nonlinear material behavior, finite elements and computational mechanics in material research, theoretical and numerical considerations of the failure process in brittle and ductile materials, and fracture mechanics.
E-mail: panos@umbc.edu

SHAO Yimin, born in 1963, is a full professor at *State Key Laboratory of Mechanical Transmission, Chongqing University, Chongqing, China*. His research interests include machine dynamic analysis, vibration analysis, signal processing, and online machinery condition monitoring and fault diagnosis systems.
Tel: +86-23-65112520; E-mail: ymshao@cqu.edu.cn

XU Yongfeng, born in 1985, is currently a PhD candidate at *Department of Mechanical Engineering, University of Maryland, Baltimore County, USA*. His research interests include dynamics, vibration, structural health monitoring, and experimental validation.
E-mail: yxu2@umbc.edu

WU Kai, born in 1986, is currently a PhD candidate at *Department of Mechanical Engineering, University of Maryland, Baltimore County, USA*. His research interests include dynamics, vibration, applied mechanics, numerical simulation, and experimental validation.
E-mail: wukail@umbc.edu

XIAO Huifang, born in 1984, is currently a lecturer at *National Engineering Research Center of Flat Rolling Equipment,*

University of Science and Technology Beijing, China. She received her PhD degree from *Chongqing University, China*, in 2012. Her research interests include signal processing and fault diagnosis, vibration control.
E-mail: huifangxiao@ustb.edu.cn

Appendix A: Derivation of equations of motion and matching and boundary conditions of the four-beam model in Fig. 2

The kinetic and potential energies of the four-beam model in Fig. 2 are given by

$$\begin{aligned}
 T &= \frac{\rho A_1}{2} \int_0^{X_1} [\dot{Y}_1(X, t)]^2 dX + \frac{\rho A_2}{2} \int_{X_1}^{X_2} [\dot{Y}_2(X, t)]^2 dX + \\
 &\quad \frac{\rho A_3}{2} \int_{X_1}^{X_2} [\dot{Y}_3(X, t)]^2 dX + \frac{\rho A_4}{2} \int_{X_2}^L [\dot{Y}_4(X, t)]^2 dX \\
 V &= \frac{EI_1}{2} \int_0^{X_1} [Y_1''(X, t)]^2 dX + \frac{EI_2}{2} \int_{X_1}^{X_2} [Y_2''(X, t)]^2 dX + \\
 &\quad \frac{EI_3}{2} \int_{X_1}^{X_2} [Y_3''(X, t)]^2 dX + \frac{EI_4}{2} \int_{X_2}^L [Y_4''(X, t)]^2 dX + \\
 &\quad \frac{1}{2C_1} [Y_2'(X_1, t) - Y_1'(X_1, t)]^2 + \\
 &\quad \frac{1}{2C_2} [Y_3'(X_1, t) - Y_1'(X_1, t)]^2 + \\
 &\quad \frac{1}{2C_3} [Y_4'(X_2, t) - Y_2'(X_2, t)]^2 + \\
 &\quad \frac{1}{2C_4} [Y_4'(X_2, t) - Y_3'(X_2, t)]^2,
 \end{aligned} \tag{A1}$$

where an overdot denotes the partial time derivative, a prime denotes a spatial derivative with respect to the corresponding spatial variable, and I_1 and I_4 are cross-sectional area moments of inertia of beam segments 1 and 4, respectively. The variations of the kinetic and potential energies are

$$\begin{aligned}
 \delta T &= \rho A_1 \int_0^{X_1} \dot{Y}_1(X, t) \delta \dot{Y}_1(X, t) dX + \\
 &\quad \rho A_2 \int_{X_1}^{X_2} \dot{Y}_2(X, t) \delta \dot{Y}_2(X, t) dX + \\
 &\quad \rho A_3 \int_{X_1}^{X_2} \dot{Y}_3(X, t) \delta \dot{Y}_3(X, t) dX + \\
 &\quad \rho A_4 \int_{X_2}^L \dot{Y}_4(X, t) \delta \dot{Y}_4(X, t) dX, \\
 \delta V &= EI_1 \int_0^{X_1} Y_1''(X, t) \delta Y_1''(X, t) dX + \\
 &\quad EI_2 \int_{X_1}^{X_2} Y_2''(X, t) \delta Y_2''(X, t) dX + \\
 &\quad EI_3 \int_{X_1}^{X_2} Y_3''(X, t) \delta Y_3''(X, t) dX + \\
 &\quad EI_4 \int_{X_2}^L Y_4''(X, t) \delta Y_4''(X, t) dX +
 \end{aligned}$$

$$\begin{aligned}
& \frac{1}{C_1} \left[Y_2'(X_1, t) - Y_1'(X_1, t) \right] \left[\delta Y_2'(X_1, t) - \delta Y_1'(X_1, t) \right] + \int_{t_1}^{t_2} \int_0^{X_1} \left[\rho A_1 \ddot{Y}_1(X, t) + EI_1 Y_1''''(X, t) \right] \delta Y_1(X, t) dX dt + \\
& \frac{1}{C_2} \left[Y_3'(X_1, t) - Y_1'(X_1, t) \right] \left[\delta Y_3'(X_1, t) - \delta Y_1'(X_1, t) \right] + \int_{t_1}^{t_2} \left[EI_1 Y_1''''(X_1, t) \delta Y_1(X_1, t) - EI_2 Y_2''''(X_1, t) \delta Y_2(X_1, t) - \right. \\
& \left. EI_3 Y_3''''(X_1, t) \delta Y_3(X_1, t) \right] dt + \\
& \frac{1}{C_3} \left[Y_4'(X_2, t) - Y_2'(X_2, t) \right] \left[\delta Y_4'(X_2, t) - \delta Y_2'(X_2, t) \right] + \int_{t_1}^{t_2} \left\{ EI_4 Y_4''(X_2, t) - \frac{1}{C_3} \left[Y_4'(X_2, t) - Y_2'(X_2, t) \right] - \right. \\
& \left. \frac{1}{C_4} \left[Y_4'(X_2, t) - Y_3'(X_2, t) \right] \right\} \delta Y_4'(X_2, t) dt - \\
& \frac{1}{C_4} \left[Y_4'(X_2, t) - Y_3'(X_2, t) \right] \left[\delta Y_4'(X_2, t) - \delta Y_3'(X_2, t) \right]. \tag{A2}
\end{aligned}$$

By Hamilton's principle,

$$\int_{t_1}^{t_2} (\delta T - \delta V) dt = 0, \tag{A3}$$

where t_1 and t_2 are arbitrary start and end times, substituting Eq. (A2) into Eq. (A3), applying integration by parts, and using the facts that $\delta Y_i(X, t) = 0$ at $t = t_1$ and $t = t_2$ yield

$$\begin{aligned}
& - \int_{t_1}^{t_2} \int_0^{X_1} \left[\rho A_1 \ddot{Y}_1(X, t) + EI_1 Y_1''''(X, t) \right] \delta Y_1(X, t) dX dt - \\
& \int_{t_1}^{t_2} \int_{X_1}^{X_2} \left[\rho A_2 \ddot{Y}_2(X, t) + EI_2 Y_2''''(X, t) \right] \delta Y_2(X, t) dX dt - \\
& \int_{t_1}^{t_2} \int_{X_1}^{X_2} \left[\rho A_3 \ddot{Y}_3(X, t) + EI_3 Y_3''''(X, t) \right] \delta Y_3(X, t) dX dt - \\
& \int_{t_1}^{t_2} \int_{X_2}^L \left[\rho A_4 \ddot{Y}_4(X, t) + EI_4 Y_4''''(X, t) \right] \delta Y_4(X, t) dX dt - \\
& \int_{t_1}^{t_2} \left[EI_1 Y_1'''(0, t) \delta Y_1(0, t) - EI_1 Y_1''(0, t) \delta Y_1'(0, t) \right] dt - \\
& \int_{t_1}^{t_2} \left[EI_4 Y_4''(L, t) \delta Y_4'(L, t) - EI_4 Y_4'''(L, t) \delta Y_4(L, t) \right] dt + \\
& \int_{t_1}^{t_2} \left\{ EI_2 Y_2''(X_1, t) - \frac{1}{C_1} \left[Y_2'(X_1, t) - \right. \right. \\
& \left. \left. Y_1'(X_1, t) \right] \right\} \delta Y_2'(X_1, t) dt + \\
& \int_{t_1}^{t_2} \left\{ EI_3 Y_3''(X_1, t) - \frac{1}{C_2} \left[Y_3'(X_1, t) - \right. \right. \\
& \left. \left. Y_1'(X_1, t) \right] \right\} \delta Y_3'(X_1, t) dt - \\
& \int_{t_1}^{t_2} \left\{ EI_2 Y_2''(X_2, t) - \frac{1}{C_3} \left[Y_4'(X_2, t) - \right. \right. \\
& \left. \left. Y_2'(X_2, t) \right] \right\} \delta Y_2'(X_2, t) dt - \\
& \int_{t_1}^{t_2} \left\{ EI_3 Y_3''(X_2, t) - \frac{1}{C_4} \left[Y_4'(X_2, t) - \right. \right. \\
& \left. \left. Y_3'(X_2, t) \right] \right\} \delta Y_3'(X_2, t) dt - \\
& \int_{t_1}^{t_2} \left\{ EI_1 Y_1''(X_1, t) - \frac{1}{C_1} \left[Y_2'(X_1, t) - Y_1'(X_1, t) \right] - \right. \\
& \left. \frac{1}{C_2} \left[Y_3'(X_1, t) - Y_1'(X_1, t) \right] \right\} \delta Y_1'(X_1, t) dt -
\end{aligned}$$

$$\begin{aligned}
& \frac{1}{C_4} \left[Y_4'(X_2, t) - Y_3'(X_2, t) \right] \left[\delta Y_4'(X_2, t) - \delta Y_3'(X_2, t) \right] dt - \\
& \int_{t_1}^{t_2} \left[EI_4 Y_4'''(X_2, t) \delta Y_4(X_2, t) - EI_2 Y_2'''(X_2, t) \delta Y_2(X_2, t) - \right. \\
& \left. EI_3 Y_3'''(X_2, t) \delta Y_3(X_2, t) \right] dt = 0. \tag{A4}
\end{aligned}$$

By Eq. (A4), the equations of motion of the four beam segments are

$$\begin{aligned}
\rho A_1 \frac{\partial^2 Y_1(X, t)}{\partial t^2} + EI_1 \frac{\partial^4 Y_1(X, t)}{\partial X^4} &= 0, \quad 0 < X < X_1, \\
\rho A_2 \frac{\partial^2 Y_2(X, t)}{\partial t^2} + EI_2 \frac{\partial^4 Y_2(X, t)}{\partial X^4} &= 0, \quad X_1 < X < X_2, \\
\rho A_3 \frac{\partial^2 Y_3(X, t)}{\partial t^2} + EI_3 \frac{\partial^4 Y_3(X, t)}{\partial X^4} &= 0, \quad X_1 < X < X_2, \\
\rho A_4 \frac{\partial^2 Y_4(X, t)}{\partial t^2} + EI_4 \frac{\partial^4 Y_4(X, t)}{\partial X^4} &= 0, \quad X_2 < X < L,
\end{aligned} \tag{A5}$$

and the boundary conditions of the four-beam model are

$$Y_1(0, t) = Y_1'(0, t) = Y_4''(L, t) = Y_4'''(L, t) = 0. \tag{A6}$$

By continuity of the displacements of the four-beam model at cross-sections X_1 and X_2 ,

$$\begin{aligned}
Y_1(X_1^-, t) &= Y_2(X_1^+, t), Y_1(X_1^-, t) = Y_3(X_1^+, t), \\
Y_4(X_2^+, t) &= Y_2(X_2^-, t), Y_4(X_2^+, t) = Y_3(X_2^-, t),
\end{aligned} \tag{A7}$$

which are the first four matching conditions of the four-beam model, and substituting Eq. (A7) into Eq. (A4), one obtains the other eight matching conditions at cross-sections X_1 and X_2 ,

$$\begin{aligned}
Y_2'(X_1^+, t) - Y_1'(X_1^-, t) &= C_1 EI_2 Y_2''(X_1^+, t), \\
Y_3'(X_1^+, t) - Y_1'(X_1^-, t) &= C_2 EI_3 Y_3''(X_1^+, t), \\
Y_4'(X_2^+, t) - Y_2'(X_2^-, t) &= C_3 EI_2 Y_2''(X_2^-, t), \\
Y_4'(X_2^+, t) - Y_3'(X_2^-, t) &= C_4 EI_3 Y_3''(X_2^-, t),
\end{aligned} \tag{A8}$$

$$\begin{aligned}
EI_1 Y_1''(X_1^-, t) &= \frac{1}{C_1} [Y_2'(X_1^+, t) - Y_1'(X_1^-, t)] + \\
&\quad \frac{1}{C_2} [Y_3'(X_1^+, t) - Y_1'(X_1^-, t)], \\
EI_1 Y_1'''(X_1^-, t) &= EI_2 Y_2'''(X_1^+, t) + EI_3 Y_3'''(X_1^+, t), \\
EI_4 Y_4''(X_2^+, t) &= \frac{1}{C_3} [Y_4'(X_2^+, t) - Y_2'(X_2^-, t)] + \\
&\quad \frac{1}{C_4} [Y_4'(X_2^+, t) - Y_3'(X_2^-, t)], \\
EI_4 Y_4'''(X_2^+, t) &= EI_2 Y_2'''(X_2^-, t) + EI_3 Y_3'''(X_2^-, t).
\end{aligned} \tag{A9}$$

Substituting $I_1 = I_4 = bh^3/12$, $I_2 = bh_1^3/12$, $I_3 = b(h-h_1)^3/12$, and Eq. (A8) into Eq. (A9) yields

$$\begin{aligned}
h^3 Y_1''(X_1^-, t) &= h_1^3 Y_2''(X_1^+, t) + (h-h_1)^3 Y_3''(X_1^+, t), \\
h^3 Y_1'''(X_1^-, t) &= h_1^3 Y_2'''(X_1^+, t) + (h-h_1)^3 Y_3'''(X_1^+, t), \\
h^3 Y_4''(X_2^+, t) &= h_1^3 Y_2''(X_2^-, t) + (h-h_1)^3 Y_3''(X_2^-, t), \\
h^3 Y_4'''(X_2^+, t) &= h_1^3 Y_2'''(X_2^-, t) + (h-h_1)^3 Y_3'''(X_2^-, t).
\end{aligned} \tag{A10}$$

Appendix B: Entries of matrices G_1 , G_2 , G_3 , and G_4 in Eqs. (27) and (28)

Entries of matrix G_1 in Eq. (27) are as follows:

$$\begin{aligned}
g_{1,1}^1 &= \sin \lambda_4 l, & g_{1,2}^1 &= \cos \lambda_4 l, \\
g_{1,3}^1 &= \sinh \lambda_4 l, & g_{1,4}^1 &= \cosh \lambda_4 l, \\
g_{2,1}^1 &= \sin \lambda_4 l, & g_{2,2}^1 &= \cos \lambda_4 l, \\
g_{2,3}^1 &= \sinh \lambda_4 l, & g_{2,4}^1 &= \cosh \lambda_4 l, \\
g_{3,1}^1 &= -\lambda_1^2 \sin \lambda_4 l, & g_{3,2}^1 &= -\lambda_1^2 \cos \lambda_4 l, \\
g_{3,3}^1 &= \lambda_1^2 \sinh \lambda_4 l, & g_{3,4}^1 &= \lambda_1^2 \cosh \lambda_4 l, \\
g_{4,1}^1 &= -\lambda_1^3 \cos \lambda_4 l, & g_{4,2}^1 &= \lambda_1^3 \sin \lambda_4 l, \\
g_{4,3}^1 &= \lambda_1^3 \cosh \lambda_4 l, & g_{4,4}^1 &= \lambda_1^3 \sinh \lambda_4 l, \\
g_{5,1}^1 &= \lambda_1 \cos \lambda_4 l, & g_{5,2}^1 &= -\lambda_1 \sin \lambda_4 l, \\
g_{5,3}^1 &= \lambda_1 \cosh \lambda_4 l, & g_{5,4}^1 &= \lambda_1 \sinh \lambda_4 l, \\
g_{6,1}^1 &= \lambda_1 \cos \lambda_4 l, & g_{6,2}^1 &= -\lambda_1 \sin \lambda_4 l, \\
g_{6,3}^1 &= \lambda_1 \cosh \lambda_4 l, & g_{6,4}^1 &= \lambda_1 \sinh \lambda_4 l, \\
g_{7,1}^1 &= 0, & g_{7,2}^1 &= 0, & g_{7,3}^1 &= 0, & g_{7,4}^1 &= 0, \\
g_{8,1}^1 &= 0, & g_{8,2}^1 &= 0, & g_{8,3}^1 &= 0, & g_{8,4}^1 &= 0.
\end{aligned} \tag{B1}$$

Entries of matrix G_2 in Eq. (27) are as follows:

$$\begin{aligned}
g_{1,1}^2 &= 0, & g_{1,2}^2 &= 1, & g_{1,3}^2 &= 0, & g_{1,4}^2 &= 1, \\
g_{1,5}^2 &= 0, & g_{1,6}^2 &= 0, & g_{1,7}^2 &= 0, & g_{1,8}^2 &= 0,
\end{aligned}$$

$$\begin{aligned}
g_{2,1}^2 &= 0, & g_{2,2}^2 &= 0, & g_{2,3}^2 &= 0, & g_{2,4}^2 &= 0, \\
g_{2,5}^2 &= 0, & g_{2,6}^2 &= 1, & g_{2,7}^2 &= 0, & g_{2,8}^2 &= 1, \\
g_{3,1}^2 &= 0, & g_{3,2}^2 &= -h_c^3 \lambda_2^2, & g_{3,3}^2 &= 0, & g_{3,4}^2 &= h_c^3 \lambda_2^2, \\
g_{3,5}^2 &= 0, & g_{3,6}^2 &= -(1-h_c)^3 \lambda_2^2, & g_{3,7}^2 &= 0, & g_{3,8}^2 &= (1-h_c)^3 \lambda_2^2, \\
g_{4,1}^2 &= -h_c^3 \lambda_2^2, & g_{4,2}^2 &= 0, & g_{4,3}^2 &= h_c^3 \lambda_2^2, & g_{4,4}^2 &= 0, \\
g_{4,5}^2 &= -(1-h_c)^3 \lambda_2^2, & g_{4,6}^2 &= 0, & g_{4,7}^2 &= (1-h_c)^3 \lambda_2^2, & g_{4,8}^2 &= 0, \\
g_{5,1}^2 &= \lambda_2, & g_{5,2}^2 &= c_1 (h_c)^3 \lambda_2^2, & g_{5,3}^2 &= \lambda_2, & g_{5,4}^2 &= -c_1 (h_c)^3 \lambda_2^2, \\
g_{5,5}^2 &= 0, & g_{5,6}^2 &= 0, & g_{5,7}^2 &= 0, & g_{5,8}^2 &= 0, \\
g_{6,1}^2 &= \lambda_3, & g_{6,2}^2 &= c_2 (1-h_c)^3 \lambda_3^2, & g_{6,3}^2 &= \lambda_3, \\
g_{6,4}^2 &= -c_2 (1-h_c)^3 \lambda_3^2, \\
g_{6,5}^2 &= 0, & g_{6,6}^2 &= 0, & g_{6,7}^2 &= 0, & g_{6,8}^2 &= 0, \\
g_{7,1}^2 &= \sin \lambda_2 l_2, & g_{7,2}^2 &= \cos \lambda_2 l_2, \\
g_{7,3}^2 &= \sinh \lambda_2 l_2, & g_{7,4}^2 &= \cosh \lambda_2 l_2, \\
g_{7,5}^2 &= -\sin \lambda_3 l_3, & g_{7,6}^2 &= -\cos \lambda_3 l_3, \\
g_{7,7}^2 &= -\sinh \lambda_3 l_3, & g_{7,8}^2 &= -\cosh \lambda_3 l_3, \\
g_{8,1}^2 &= \lambda_2 \cos \lambda_2 l_2 - [c_3 (h_c)^3 - c_4 (1-h_c)^3] h_c^3 \lambda_2^2 \sin \lambda_2 l_2, \\
g_{8,2}^2 &= -\lambda_2 \sin \lambda_2 l_2 - [c_3 (h_c)^3 - c_4 (1-h_c)^3] h_c^3 \lambda_2^2 \cos \lambda_2 l_2, \\
g_{8,3}^2 &= \lambda_2 \cosh \lambda_2 l_2 + [c_3 (h_c)^3 - c_4 (1-h_c)^3] h_c^3 \lambda_2^2 \sinh \lambda_2 l_2, \\
g_{8,4}^2 &= \lambda_2 \sinh \lambda_2 l_2 + [c_3 (h_c)^3 - c_4 (1-h_c)^3] h_c^3 \lambda_2^2 \cosh \lambda_2 l_2, \\
g_{8,5}^2 &= -\lambda_3 \cos \lambda_3 l_3 - \\
&\quad [c_3 (h_c)^3 - c_4 (1-h_c)^3] (1-h_c)^3 \lambda_3^2 \sin \lambda_3 l_3, \\
g_{8,6}^2 &= \lambda_3 \sin \lambda_3 l_3 - [c_3 (h_c)^3 - c_4 (1-h_c)^3] (1-h_c)^3 \lambda_3^2 \cos \lambda_3 l_3, \\
g_{8,7}^2 &= -\lambda_3 \cosh \lambda_3 l_3 + \\
&\quad [c_3 (h_c)^3 - c_4 (1-h_c)^3] (1-h_c)^3 \lambda_3^2 \sinh \lambda_3 l_3, \\
g_{8,8}^2 &= -\lambda_3 \sinh \lambda_3 l_3 + \\
&\quad [c_3 (h_c)^3 - c_4 (1-h_c)^3] (1-h_c)^3 \lambda_3^2 \cosh \lambda_3 l_3.
\end{aligned} \tag{B2}$$

Entries of matrix G_3 in Eq. (28) are as follows:

$$\begin{aligned}
g_{1,1}^3 &= \sin \lambda_2 l_2, & g_{1,2}^3 &= \cos \lambda_2 l_2, \\
g_{1,3}^3 &= \sinh \lambda_2 l_2, & g_{1,4}^3 &= \cosh \lambda_2 l_2, \\
g_{1,5}^3 &= \sin \lambda_3 l_3, & g_{1,6}^3 &= \cos \lambda_3 l_3, \\
g_{1,7}^3 &= \sinh \lambda_3 l_3, & g_{1,8}^3 &= \cosh \lambda_3 l_3, \\
g_{2,1}^3 &= -h_c^3 \lambda_2^2 \sin \lambda_2 l_2 - h_c^3 \lambda_2^2 \cos \lambda_2 l_2, \\
g_{2,2}^3 &= -h_c^3 \lambda_2^2 \cos \lambda_2 l_2 + h_c^3 \lambda_2^2 \sin \lambda_2 l_2, \\
g_{2,3}^3 &= h_c^3 \lambda_2^2 \sinh \lambda_2 l_2 + h_c^3 \lambda_2^2 \cosh \lambda_2 l_2, \\
g_{2,4}^3 &= h_c^3 \lambda_2^2 \cosh \lambda_2 l_2 + h_c^3 \lambda_2^2 \sinh \lambda_2 l_2, \\
g_{2,5}^3 &= -(1-h_c)^3 \lambda_2^2 \sin \lambda_3 l_3 - (1-h_c)^3 \lambda_2^2 \cos \lambda_3 l_3,
\end{aligned}$$

$$\begin{aligned}
g_{2,6}^3 &= -(1-h_c)^3 \lambda_3^2 \cos \lambda_3 l_3 + (1-h_c)^3 \lambda_3^3 \sin \lambda_3 l_3, \\
g_{2,7}^3 &= (1-h_c)^3 \lambda_3^2 \sinh \lambda_3 l_3 + (1-h_c)^3 \lambda_3^3 \cosh \lambda_3 l_3, \\
g_{2,8}^3 &= (1-h_c)^3 \lambda_3^2 \cosh \lambda_3 l_3 + (1-h_c)^3 \lambda_3^3 \sinh \lambda_3 l_3, \\
g_{3,1}^3 &= \lambda_2 \cos \lambda_2 l_2, \quad g_{3,2}^3 = -\lambda_2 \sin \lambda_2 l_2, \\
g_{3,3}^3 &= \lambda_2 \cosh \lambda_2 l_2, \quad g_{3,4}^3 = \lambda_2 \sinh \lambda_2 l_2, \\
g_{3,5}^3 &= \lambda_3 \cos \lambda_3 l_3, \quad g_{3,6}^3 = -\lambda_3 \sin \lambda_3 l_3, \\
g_{3,7}^3 &= \lambda_3 \cosh \lambda_3 l_3, \quad g_{3,8}^3 = \lambda_3 \sinh \lambda_3 l_3, \\
g_{4,1}^3 &= 0, \quad g_{4,2}^3 = 0, \quad g_{4,3}^3 = 0, \quad g_{4,4}^3 = 0, \\
g_{4,5}^3 &= 0, \quad g_{4,6}^3 = 0, \quad g_{4,7}^3 = 0, \quad g_{4,8}^3 = 0.
\end{aligned}$$

(B3)

Entries of matrix \mathbf{G}_4 in Eq. (28) are

$$\begin{aligned}
g_{1,1}^4 &= 0, \quad g_{1,2}^4 = 2, \quad g_{1,3}^4 = 0, \quad g_{1,4}^4 = 2, \\
g_{2,1}^4 &= -\lambda_4^3, \quad g_{2,2}^4 = -\lambda_4^2, \quad g_{2,3}^4 = \lambda_4^3, \quad g_{2,4}^4 = \lambda_4^2, \\
g_{3,1}^4 &= 2\lambda_4, \quad g_{3,2}^4 = \left(c_3 (h_c)^3 + c_4 (1-h_c)^3\right) \lambda_4^2, \\
g_{3,3}^4 &= 2\lambda_4, \quad g_{3,4}^4 = -\left(c_3 (h_c)^3 + c_4 (1-h_c)^3\right) \lambda_4^2, \\
g_{4,1}^4 &= -\lambda_4^2 \sin \lambda_4 l_4 - \lambda_4^3 \cos \lambda_4 l_4, \\
g_{4,2}^4 &= -\lambda_4^2 \cos \lambda_4 l_4 + \lambda_4^3 \sin \lambda_4 l_4, \\
g_{4,3}^4 &= \lambda_4^2 \sinh \lambda_4 l_4 + \lambda_4^3 \cosh \lambda_4 l_4, \\
g_{4,4}^4 &= \lambda_4^2 \cosh \lambda_4 l_4 + \lambda_4^3 \sinh \lambda_4 l_4.
\end{aligned} \tag{B4}$$